



Void growth and coalescence in triaxial stress fields in irradiated FCC single crystals



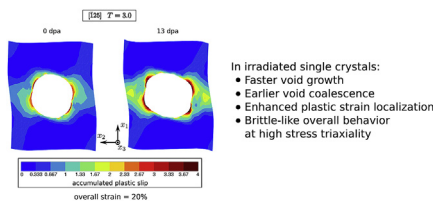
Chao Ling^{a, b}, Benoît Tanguy^{a, *}, Jacques Besson^b, Samuel Forest^b, Felix Latourte^c

^a DEN – Service d'Etudes des Matériaux Irradiés, CEA, Université Paris–Saclay, F-91191 Gif-sur-Yvette cedex, France

^b MINES ParisTech, PSL Research University, MAT – Centre des matériaux, CNRS UMR 7633, BP 87 91003 Evry, France

^c EDF R&D, MMC, Site des Renardières, F-77818 Moret-sur-Loing cedex, France

GRAPHICAL ABSTRACT



ARTICLE INFO

Article history:

Received 4 November 2016

Received in revised form

31 March 2017

Accepted 10 April 2017

Available online 19 April 2017

Keywords:

Porous single crystals

Void coalescence

Void growth

Irradiation effects

ABSTRACT

Void growth and coalescence, known as main mechanisms of ductile fracture, are investigated for irradiated FCC single crystals. Finite element simulations of voided unit cells are performed with a single crystal plasticity model accounting for strain hardening and softening associated with irradiation-induced defects. The simulations predict a rather brittle overall behavior for the voided irradiated single crystal at high stress triaxiality, with a large amount of local plastic deformation, which is consistent with experimental observations reported in the literature for stainless steels irradiated in fast reactors. Compared with unirradiated single crystals, irradiated crystals exhibit a higher void growth rate leading to an earlier void coalescence, which is caused by a stronger plastic slip localization in the region near the voids.

© 2017 Elsevier B.V. All rights reserved.

1. Introduction

Neutron irradiation of stainless steels leads to drastic modifications of mechanical properties, e.g., increase in yield stress, decrease in ductility (uniform elongation) and decrease of strain hardening capacity [1–3]. The changes of the mechanical properties depend on various parameters (virgin properties of steels, irradiation temperature, irradiation spectrum, etc.) and are associated with defect clusters induced by irradiation, such as Frank

loops, precipitates, vacancies and black dots [4–6]. Moreover, neutron irradiation at low temperature generally causes a reduction in fracture toughness of stainless steels ([7,8] and references therein). However, ductile fracture remains the dominant fracture mechanism (see, e.g., [8–11]) especially for the steels irradiated up to about 10–20 displacements per atom (dpa), even though non-ductile modes have also been observed. Little [9] revealed a significant loss of fracture toughness in solution treated Type 321 austenitic stainless steels after irradiation in Dounreay Fast Reactor up to 43 dpa. The author found that the ductile mode was the primary fracture mechanism after irradiation and that the ductile dimples were much finer, initiating from irradiation-induced micro-sized TiC precipitates. Fukuya et al. [10] showed different

* Corresponding author.

E-mail address: benoit.tanguy@cea.fr (B. Tanguy).

fracture modes (ductile and non-ductile) under impact and tensile tests for cold-worked 316 stainless steels irradiated up to 73 dpa in a pressurized water reactor. The ductile mode corresponds to void growth and coalescence with very small final dimples (about 1 μm). The non-ductile mode corresponds to intergranular fracture. In the impact tests, purely ductile and ductile dominant modes were observed on the steels irradiated up to 22 dpa and tested at 30 °C and 150 °C. In the tensile tests with $1.1 \times 10^{-4}\text{s}^{-1}$ strain rate, the steels tested at 320 °C displayed ductile fracture mode with up to 73 dpa irradiation damage. Neustroev and Garner [11] investigated fracture behavior of a titanium-stabilized stainless steel cut from fuel pin claddings and fuel assembly wrappers of the fast reactor BOR-60. The authors reported a transgranular cup-cone fracture morphology for tensile specimens extracted from assembly wrappers with high swelling (30%). The fracture surface exhibited fine dimples which implied that failure proceeded by micropore coalescence. They emphasized the large amount of local deformation at the failure site, despite the highly reduced elongation at the macroscopic level. Margolin et al. [8] studied fracture mechanisms in titanium-stabilized austenitic steels taken from shield assemblies of BOR-60 reactor. The authors observed dimple fracture with voids of size 2–10 μm nucleated from Ti carbonitrides for limited swelling cases (swelling < 2% and irradiation damage up to 80–150 dpa). They also reported dimple fracture by growth and coalescence of very small swelling voids (about 20 nm) for relatively high swelling level (5–6%). These experimental observations clearly demonstrate that ductile fracture occurs in irradiated stainless steels for various irradiation conditions. It is hence of great importance to develop models to describe ductile fracture processes in these materials.

So far, few studies have been devoted to the modeling of ductile fracture in irradiated steels. An attempt was made by Margolin and his co-workers based on their continuous model developed for fracture by void nucleation and growth in polycrystalline materials [12]. They have proposed an improved version of the model to predict fracture toughness and fracture strain of irradiated austenitic steels accounting for stress triaxiality and irradiation swelling [13,14]. The authors consider voids resulting from swelling and voids nucleated from inclusions during plastic straining [8]. The first are small and embedded inside grains. In addition, it was shown in Ref. [9] that ductile fracture in irradiated stainless steels may also occur by void nucleation from irradiation-induced micro-sized TiC precipitates. In all these cases, voids are smaller than a grain. Therefore, it is important to consider void growth at the scale of a single crystal (i.e., voids embedded in a grain) in the modeling of ductile rupture. It has been shown in Refs. [15,16] that crystallographic orientation has a significant effect on void growth and coalescence in single crystals. Besides, deformation mechanisms in the irradiated steels change due to irradiation-induced defects. In particular, strong softening at the onset of plastic yielding has been observed in irradiated materials (see, e.g. Refs. [2,3]). Softening may have an impact on the growth and coalescence of voids as shown using unit cell calculation in the case of glassy polymers [17,18] and rubber-toughened glassy polymers [19,20]. These studies evidenced the localization of plastic flow in the intervoid ligament of the polymers due to softening.

In the present study, we aim at studying growth and coalescence of pre-existing voids leading to transgranular ductile fracture of irradiated austenitic stainless steels. These voids have a typical size of about 20 nm and lie within the crystallographic grains. In the unirradiated material voids leading to ductile fracture are initiated at relatively large inclusions (few μm) such as Ti carbonitrides (stainless steels) or manganese sulfides (low carbon steels). These primary defects are not considered in this work which focuses on secondary voids caused by high irradiation levels. Other fracture

mechanisms observed in austenitic stainless steels irradiated up to high damage dose are not considered, e.g. channel fracture [8,9] and intergranular fracture [10]. To this end, void growth and coalescence in single crystals are simulated by finite element method within a finite strain framework of single crystal plasticity. Irradiated and unirradiated single crystals are considered. The effect of post-irradiation hardening on void growth and coalescence is evaluated. To the authors' knowledge, these are the first simulations of void growth and coalescence in irradiated single crystals. The paper is organized as follows. The FE formulation of the simulation is described in section 2, followed by the single crystal plasticity model accounting for the irradiation-induced defects in section 3. Results of the simulations are presented and discussed in section 4. Conclusions are drawn in section 5.

Throughout this paper, scalars, vectors, second order tensors and fourth order tensors are denoted respectively by a , \underline{a} , $\underline{\underline{a}}$ and $\underline{\underline{\underline{a}}}$. Simple and double contractions are written as $\underline{a} \cdot \underline{b}$, $\underline{a} : \underline{b}$, and $\underline{\underline{a}} : \underline{\underline{b}}$, and tensor product as $\underline{\underline{a}} \otimes \underline{\underline{b}}$. With the components expressed in a Cartesian coordinate system with an orthonormal basis ($\mathbf{e}_1, \mathbf{e}_2, \mathbf{e}_3$), the tensorial notation can be expressed as $\underline{a} \cdot \underline{b} = a_i b_i$, $\underline{a} : \underline{b} = a_{ij} b_{ij}$, $\underline{\underline{a}} : \underline{\underline{b}} = a_{ijkl} b_{kl}$, and $\underline{\underline{a}} \otimes \underline{\underline{b}} = a_i b_j$, where repeated indices are summed.

2. Unit cell simulations

Ductile fracture of metals and alloys at moderate to high stress triaxiality (the ratio of the mean stress to the von Mises equivalent stress) is well-known to be controlled by void nucleation, growth and coalescence. Since the seminal works by McClintock [21], Rice and Tracey [22] and Gurson [23], numerous studies have been investigating ductile fracture by different approaches relying on experimental, analytical and numerical methods. Readers are referred to the recent reviews in Refs. [24–26] for more details. Among the possible methods, Unit Cell (UC) Finite Element (FE) computations, performed on a representative volume element with one or several voids, are widely used. After the pioneering work of Needleman [27], UC simulations have allowed the study of ductile fracture process (see, e.g., [28,29] for void nucleation, [30,31] for void growth and coalescence), to assess and calibrate phenomenological or physically based models (see, e.g., [32,33]).

In this study, the UC model is used to analyze growth and coalescence of pre-existing voids in single crystals. The voids can either be nucleated from irradiation-induced precipitates or be swelling voids. These two kinds of voids are not distinguished. The FE formulation of the problem is similar to that of Ling et al. [16] and it is briefly reviewed in the following. The simulations are performed within a finite strain framework for single crystal plasticity based on the multiplicative decomposition of the deformation gradient F . The constitutive equations will be described in the next section.

2.1. FE formulation

The simulations are performed with the FE software Zset [34,35]. Throughout the paper, variables at microscopic and macroscopic scale are distinguished. The variables with an overline symbol (e.g., \overline{F}) are used for macroscopic scale at which an effective behavior of the unit cell is observed, while the variables without the overline symbol describe the behavior at the microscopic scale, i.e., at each material point inside the unit cell.

The problem setup is shown in Fig. 1. It is assumed that the distribution of voids in the single crystal is homogeneous. Thus, a unit cell, i.e., a representative elementary volume, Ω_0^{tot} can be considered as a cube of length L_0 with a spherical void of radius R_0 at its center (see Fig. 2a). Notice that L_0 characterizes the average distance between voids. Thus, the initial void volume fraction f_0 is

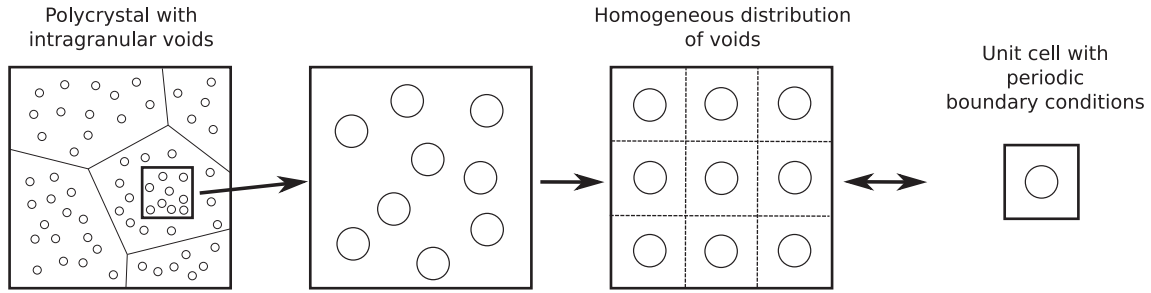


Fig. 1. Problem setup for unit cell simulations.

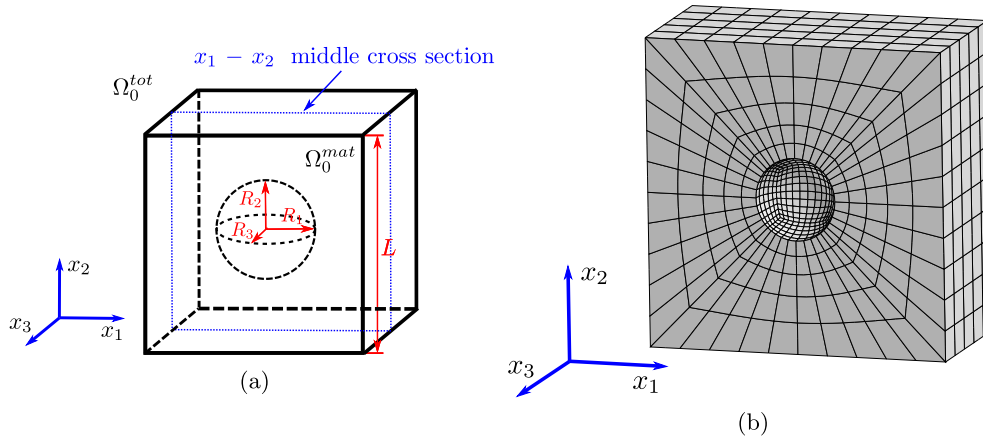


Fig. 2. Unit cell: (a) the geometry, (b) half of the FE mesh with $f_0 = 0.01$.

$$f_0 = \frac{4}{3} \pi \frac{R_0^3}{L_0^3}. \quad (1)$$

The edges of the unit cell are initially parallel to the Cartesian coordinate x_i -axes.

The unit cell is meshed with reduced-integration quadratic hexahedral elements (see Fig. 2b). Numerical periodic homogenization at finite strains is used for the simulations and the elements are enhanced by introducing average strains (\bar{F}_{ij}) as degrees of freedom. The unit cell is subjected to periodic boundary conditions expressed by:

$$\mathbf{u} = \bar{\mathbf{F}} \cdot \mathbf{X} + \mathbf{v}, \quad (2)$$

where $\bar{\mathbf{F}}$ denotes the macroscopic deformation gradient, \mathbf{u} the displacement vector and \mathbf{v} a periodic fluctuation vector which obey the following periodicity condition:

$$\mathbf{v}(\mathbf{x}^+) = \mathbf{v}(\mathbf{x}^-) \quad (3)$$

where \mathbf{x}^+ and \mathbf{x}^- denote the position of homologous nodes on opposite faces of the unit cell. The use of periodic boundary conditions implies that fracture is investigated at the microstructural level (failure by internal necking in the present case) so that plastic localization which occurs at a structural level (e.g. diffuse necking or shear band localization) cannot be directly predicted by the approach. The constitutive relations derived from the unit cell analyses such as the Gurson-like model proposed in Refs. [16,36] can however be applied at the structural level.

The microscopic first Piola–Kirchhoff stress tensor $\underline{\mathcal{S}}$ and the

associated macroscopic tensor $\bar{\mathcal{S}}$ are related by

$$\bar{\mathcal{S}} = \frac{1}{V_0^{\text{tot}}} \int_{\Omega_0^{\text{tot}}} \underline{\mathcal{S}} dV_0 = (1 - f_0) \frac{1}{V_0^{\text{mat}}} \int_{\Omega_0^{\text{mat}}} \underline{\mathcal{S}} dV_0, \quad (4)$$

where V_0^{tot} and V_0^{mat} denote respectively the total volume of the unit cell and the volume of the matrix in the reference configuration. In uniaxial tension, the first Piola–Kirchhoff stress corresponds to the so-called engineering stress.

The macroscopic Cauchy stress tensor $\bar{\boldsymbol{\sigma}}$ is related to the macroscopic first Piola–Kirchhoff stress tensor by:

$$\bar{\boldsymbol{\sigma}} = \frac{1}{J} \bar{\mathcal{S}} \cdot \bar{\mathbf{F}}^T, \quad (5)$$

with $J = \det(\bar{\mathbf{F}})$. The Cauchy stress tensor corresponds to the true stress in the uniaxial tension case.

The microscopic deformation gradient $\underline{\mathbf{F}}$ and the macroscopic tensor $\bar{\mathbf{F}}$ are related by:

$$\bar{\mathbf{F}} = \frac{1}{V_0^{\text{tot}}} \int_{\Omega_0^{\text{tot}}} \underline{\mathbf{F}} dV_0. \quad (6)$$

Constant macroscopic Cauchy stress triaxiality T is imposed with

$$\bar{\boldsymbol{\sigma}} = \begin{bmatrix} \bar{\sigma}_{11} & 0 & 0 \\ 0 & \bar{\sigma}_{22} & 0 \\ 0 & 0 & \bar{\sigma}_{33} \end{bmatrix} = \bar{\sigma}_{11} \begin{bmatrix} 1 & 0 & 0 \\ 0 & \eta_2 & 0 \\ 0 & 0 & \eta_3 \end{bmatrix} = \bar{\sigma}_{11} \bar{\boldsymbol{\sigma}}_0 \quad (7)$$

with

$$\eta_2 = \frac{\bar{\sigma}_{22}}{\bar{\sigma}_{11}}, \eta_3 = \frac{\bar{\sigma}_{33}}{\bar{\sigma}_{11}}, 0 \leq \eta_2, \eta_3 \leq 1, \quad (8)$$

such that

$$T = \frac{\bar{\sigma}_m}{\bar{\sigma}_{eq}} = \frac{1 + \eta_2 + \eta_3}{3\sqrt{1 - \eta_2 - \eta_3 - \eta_2\eta_3 + \eta_2^2 + \eta_3^2}}. \quad (9)$$

Only axisymmetric loadings are considered here, which implies that $\eta_2 = \eta_3 = \eta$ and that the imposed macroscopic Cauchy stress triaxiality is

$$T = \frac{1 + 2\eta}{3(1 - \eta)}. \quad (10)$$

The method used to impose a constant triaxiality is described in Ref. [16]. In the simulation, an initial void volume fraction equal to $f_0 = 0.01$ is considered. In most engineering materials the volume fraction of inclusions leading to void nucleation is much smaller (typically in the range 10^{-4} to 10^{-3}). However swelling due to irradiation can cause a volume increase up to 0.1 (see e.g. Ref. [37]) so that $f_0 = 0.01$ corresponds to intermediate swelling. Moderate to high stress triaxialities are investigated (see Table 1). These relatively high stress triaxialities correspond to those encountered in ductile failure process zones, such as in the vicinity of a crack tip.

3. Single crystal plasticity model

Crystal plasticity models accounting for the irradiation-induced degradation of mechanical properties of metals and alloys have recently been developed, such as that of Xiao et al. [38] for Fe-Cr alloys, Barton et al. [39], Hu et al. [40] and Xiao et al. [41] for iron, Arsenlis et al. [42], Rahul and De [43] and Xiao et al. [44] for copper, and Patra and McDowell [45,46] for ferritic/martensitic steels. The model used in the present study was developed in the work of Han [47] for austenitic stainless steels irradiated in PWR's conditions and then used by Hure et al. [48] for studying the intergranular stress distribution in irradiated stainless steels. The influence of irradiation-induced microstructural defects on strain hardening and softening is taken into account in the model. The model is developed within a finite strain framework. It accounts for the effect of irradiation dose on the hardening/softening law in post-irradiation testing.

3.1. Kinematics

The framework is based on the multiplicative decomposition of the deformation gradient $\underline{\underline{F}}$ [49,50] (see Fig. 3):

$$\underline{\underline{F}} = \underline{\underline{E}} \cdot \underline{\underline{P}}, \quad (11)$$

with the elastic part $\underline{\underline{E}}$ and the plastic part $\underline{\underline{P}}$. It is assumed that the crystal deforms by gliding of dislocations on prescribed slip planes with the normal $\underline{\underline{n}}^s$ in the direction $\underline{\underline{m}}^s$ ($s = 1, 2, \dots, N$). A lattice orientation, specified by the directors $\underline{\underline{n}}^s$ and $\underline{\underline{m}}^s$, is attributed to each material point. The lattice direction is the same in the initial configuration C_0 and in the intermediate configuration C_i .

The velocity gradient $\underline{\underline{L}}$ can be decomposed into two parts:

Table 1
Values of the stress triaxiality T and corresponding η used in the simulations.

η	0.4	0.538	0.625	0.727
T	1.0	1.5	2.0	3.0

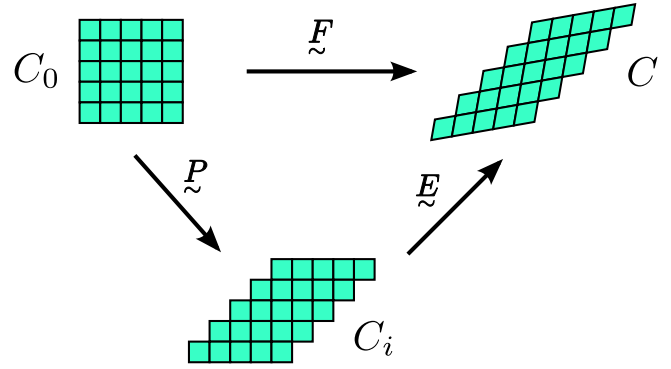


Fig. 3. Multiplicative decomposition of the deformation gradient.

$$\underline{\underline{L}} = \underline{\underline{\dot{F}}} \cdot \underline{\underline{F}}^{-1} = \underline{\underline{L}}^e + \underline{\underline{E}} \cdot \underline{\underline{L}}^p \cdot \underline{\underline{E}}^{-1}, \quad (12)$$

with the elastic part of the velocity gradient $\underline{\underline{L}}^e$ in the current configuration C

$$\underline{\underline{L}}^e = \underline{\underline{\dot{E}}} \cdot \underline{\underline{E}}^{-1}, \quad (13)$$

and the plastic part of the velocity gradient $\underline{\underline{L}}^p$ in the intermediate configuration C_i

$$\underline{\underline{L}}^p = \underline{\underline{\dot{P}}} \cdot \underline{\underline{P}}^{-1}. \quad (14)$$

3.2. Definition of stresses

According to Mandel's approach [50] (see also [51,52]), stress tensors are defined as follows.

The second Piola–Kirchhoff stress tensor $\underline{\underline{\Pi}}^e$, defined with respect to the intermediate configuration C_i , is given by

$$\underline{\underline{\Pi}}^e = J_e \underline{\underline{E}}^{-1} \cdot \underline{\underline{\sigma}} \cdot \underline{\underline{E}}^{-T}, \quad (15)$$

where $\underline{\underline{\sigma}}$ is the Cauchy stress defined in the current configuration C and J_e is the determinant of the tensor $\underline{\underline{E}}$.

The elastic Green–Lagrange strain tensor $\underline{\underline{E}}_{GL}^e$ is defined as

$$\underline{\underline{E}}_{GL}^e = \frac{1}{2} \left(\underline{\underline{E}}^T \cdot \underline{\underline{E}} - \underline{\underline{1}} \right). \quad (16)$$

$\underline{\underline{\Pi}}^e$ is related to $\underline{\underline{E}}_{GL}^e$ by the elasticity law:

$$\underline{\underline{\Pi}}^e = \underline{\underline{C}} : \underline{\underline{E}}_{GL}^e, \quad (17)$$

where $\underline{\underline{C}}$ is the fourth-order anisotropic elasticity tensor, which can be expressed in terms of three parameters C_{11} , C_{12} and C_{44} for cubic elasticity.

In addition, the driving force for single crystal plasticity is known as the Mandel stress $\underline{\underline{M}}$, which is the work-conjugate to $\underline{\underline{L}}^p$ in the intermediate configuration:

$$\underline{\underline{M}} = J_e \underline{\underline{E}}^T \cdot \underline{\underline{\sigma}} \cdot \underline{\underline{E}}^{-T} = \underline{\underline{E}}^T \cdot \underline{\underline{E}} \cdot \underline{\underline{\Pi}}^e. \quad (18)$$

3.3. Flow rule

For each slip system s , a yield function can be defined as:

$$\phi^s = |\tau^s| - \tau_c^s, \quad (19)$$

where τ^s is the resolved shear stress and τ_c^s is the critical resolved shear stress (CRSS). τ^s is defined with the Mandel stress:

$$\tau^s = \underline{\mathbf{M}} : \underline{\mathbf{N}}^s, \quad (20)$$

where $\underline{\mathbf{N}}^s$ denotes the Schmid tensor with $\underline{\mathbf{N}}^s = \underline{\mathbf{m}}^s \otimes \underline{\mathbf{n}}^s$. For each slip system, yielding occurs for $\phi^s \geq 0$. The plastic strain rate $\underline{\mathbf{L}}^p$ can be defined as

$$\underline{\mathbf{L}}^p = \underline{\dot{\mathbf{P}}} \cdot \underline{\mathbf{P}}^{-1} = \sum_{s=1}^N \text{sign}(\tau^s) \dot{\gamma}^s \underline{\mathbf{N}}^s, \quad (21)$$

with the total number of slip systems N and the plastic slip rate $\dot{\gamma}^s$ given by

$$\dot{\gamma}^s = \dot{\gamma}_{\text{ref}} \left\langle \frac{\phi^s}{\tau_{\text{ref}}^s} \right\rangle^n, \quad (22)$$

where $\dot{\gamma}_{\text{ref}}$ is a reference slip rate and τ_{ref}^s is a reference resolved shear stress. Note that $\langle \bullet \rangle = \bullet$ if $\bullet > 0$, else $\langle \bullet \rangle = 0$.

3.4. Hardening rule

The slip resistance τ_c^s , i.e., the critical resolved shear stress, on a particular slip system s is decomposed into a thermal part τ_T^s and an athermal part τ_A^s :

$$\tau_c^s = \tau_T^s + \tau_A^s. \quad (23)$$

τ_T^s corresponds to lattice friction which is dependent on temperature and assumed to be constant at a given temperature. τ_A^s represents the athermal contribution of the flow stress. Three terms are considered to contribute to the athermal slip resistance for the irradiated material:

$$\tau_A^s = \underbrace{\mu b_D \sqrt{\sum_u^{12} a^{su} \rho_D^u}}_{\text{dislocation term}} + \underbrace{\alpha_L \mu b_L \sqrt{\sum_p^4 \phi_L \rho_L^p}}_{\text{loop term}} + \underbrace{\tau_a \exp\left(-\frac{\gamma^s}{\gamma_0}\right)}_{\text{unpinning term}}, \quad (24)$$

where b_D is the norm of the Burgers vector of dislocations, μ the shear modulus, ρ_D^u the dislocation density of system u , a^{su} the matrix of long-range interactions between dislocations, α_L a parameter setting the relative contribution of Frank loops to the hardening, b_L the norm of the Burgers vector of Frank loops, ϕ_L the mean diameter of Frank loops, ρ_L^p the density of Frank loops in the slip plane p , τ_a a reference shear stress for dislocation unpinning and γ_0 a coefficient to adjust the avalanche speed after unpinning the dislocations. The form of interaction matrix a^{su} is given in Appendix A for FCC crystals.

The first term (called the dislocation term in the following) on the right-hand side of eq. (24) is the slip resistance provided by the interaction of dislocation network [53]. The second term (loop term) accounts for the effect of Frank loops generated by irradiation impeding dislocation motion. Based on Mughrabi's observation [54] that the junction energy of dislocations and loops is significantly greater than that of thermal activation, the hardening due to Frank loops is considered to contribute to the athermal part. The third term (unpinning term) is introduced based on the observation

by Tanguy et al. [55] that the hardening effect is under-estimated if only the hardening due to Frank loops is considered as a dispersed barrier hardening. This unpinning term aims at modeling the static ageing effects arising once irradiation defect cascades are present in the material microstructure [56–58]. For the unirradiated material, only the dislocation term is considered.

The description of the evolution of dislocation densities is based on two mechanisms: the multiplication and the annihilation of dislocations [59–63]. The dislocation density ρ_D^s follows:

$$\dot{\rho}_D^s = \frac{1}{b_D} \left(\frac{1}{L^s} - g_c \rho_D^s \right) \dot{\gamma}^s, \quad (25)$$

where L^s is the mean free path of the dislocation segment before being stopped at obstacles in the form of forest dislocations and g_c is the critical distance controlling the annihilation of dislocations with opposite signs. For unirradiated crystals, L^s is written as

$$L^s = L_D^s = \frac{\kappa}{\sqrt{\sum_u^{12} b^{su} \rho_D^u}}. \quad (26)$$

The κ parameter is proportional to the number of obstacles crossed by a dislocation before being pinned. The matrix b^{su} describes the interaction between dislocations; it has the same form as the interaction matrix a^{su} (see Appendix A). In irradiated stainless steels, Frank loops are not rigid obstacles. Molecular dynamics simulations [64] showed that Frank loops can interact with dislocations, resulting in the unfauling of the loops. According to Yang et al. [65], dislocations can be emitted from the circumference of the loop during the interaction. These results motivate the modification of the mean free path L^s in order to include the influence of Frank loops; it is assumed to take the following form:

$$\frac{1}{L^s} = \frac{1}{L_D^s} + \frac{1}{L_L}, \quad (27)$$

where L_D^s is still given by eq. (26) and the Frank loop contribution to the mean free path writes

$$L_L = \frac{\kappa}{\sqrt{k_{dl} \sum_p^4 \phi_L \rho_L^p}}, \quad (28)$$

where k_{dl} is a coefficient setting the effective interaction between Frank loops and dislocations.

The model proposed by Krishna and his co-workers [66,67] is adopted to describe the evolution of Frank loop densities. It is based on the mechanism of annihilation of Frank loops by dislocations gliding in the loop's plane. The probability and frequency of the annihilation of a Frank loop are taken into account. The decrease rate of Frank loop density $\dot{\rho}_L^p$ on plane p is

$$\dot{\rho}_L^p = -A \left(\sum_{s \in \text{plane}(p)} \rho_D^s \right) \frac{\phi_L}{b_D} (\rho_L^p - \rho_L^{\text{sat}}) \left(\sum_{s \in \text{plane}(p)} \dot{\gamma}^s \right), \quad (29)$$

where A denotes the annihilation area and ρ_L^{sat} the stabilized effective density of Frank loops. $s \in \text{plane}(p)$ represents all the dislocation slip systems having the same slip plane as the Frank loop p .

4. Results and discussions

FCC single crystal lattice is considered with 12 dislocation slip systems ($N = 12$) specified by the slip direction vector $\underline{\mathbf{m}}^s$ and the normal vector $\underline{\mathbf{n}}^s$ to the slip plane (see Table 2). Frank loops are

Table 2
Slip systems in FCC single crystals. The labels are given according to the Schmid–Boas convention [70].

s	1	2	3	4	5	6	7	8	9	10	11	12
label	B4	B2	B5	D4	D1	D6	A2	A6	A3	C5	C3	C1
\mathbf{m}^s		(111)			($\bar{1}\bar{1}1$)			($\bar{1}11$)			($\bar{1}\bar{1}1$)	
\mathbf{m}^s	$[\bar{1}01]$	$[0\bar{1}1]$	$[\bar{1}10]$	$[\bar{1}01]$	$[011]$	$[110]$	$[0\bar{1}1]$	$[110]$	$[101]$	$[\bar{1}10]$	$[101]$	$[011]$

supposed to remain on the four {111} dislocation slip planes (see Table 3). The orientation of the cubic unit cell is characterized by the orientation of its principal axes (x_1 , x_2 and x_3 in Fig. 2a) expressed in the FCC lattice frame. Three orientations are chosen: $[100]–[010]–[001]$, $[111]–[\bar{2}11]–[0\bar{1}1]$ and $[\bar{1}25]–[1\bar{2}1]–[210]$. For the sake of brevity, the lattice direction along the principle loading direction (the axis x_1) is used to designate the crystallographic orientation, i.e., $[100]$, $[111]$ and $[\bar{1}25]$ (Table 4). The orientations correspond to different number of primary slip systems of void-free crystals in axisymmetric loading (see Table 4) and different symmetries about the coordinate planes. In uniaxial tension, $[100]$ is a multiple slip (8 primary slip systems) orientation with mirror symmetry about three coordinate planes; $[111]$ is a multiple slip (6 primary slip systems) orientation with mirror symmetry about the $x_1–x_2$ coordinate plane, and $[\bar{1}25]$ represents single slip orientation with no mirror symmetry about the coordinate planes. Note that the same primary slip systems are activated in axisymmetric loading as in uniaxial tension along axis x_1 . Schmid factors are also calculated for the three orientations in the case of uniaxial tension along axis x_1 .

The material parameters used in the simulations were identified in the work of Han [47] for 304L stainless steels irradiated up to 13 dpa. The identification of the material parameters was performed by fitting a polycrystalline aggregate FE model response to the tensile test results of Pokor et al. [2,3] at 340 °C. Among the parameters, a^{su} and b^{su} are two matrices (12×12 for FCC single crystal), describing the interaction between dislocations. Each of them is constructed by 6 independent parameters: a_1, a_2, \dots, a_6 for a^{su} and b_1, b_2, \dots, b_6 for b^{su} (see Appendix A). The values of a_i with $i = 1, 2, \dots, 6$ are obtained by discrete dislocation dynamics [68]. However, to the authors' knowledge, no study has been conducted for b_i with $i = 1, 2, \dots, 6$ and they are supposed to take the values listed in Table 5. Due to the crystal structure and to the considered slip systems, τ_i^s can be considered as having the same value for all systems. The initial dislocation density is supposed to be equal for every system. Hence, the initial value of the dislocation density for system s is $\rho_D^s|_{ini} = \rho_D^{tot}/12$, where ρ_D^{tot} is the total dislocation density measured in experiments. The same hypothesis is made for the density of Frank loops and each system has an initial value of Frank loop density following $\rho_L^p|_{ini} = \rho_L^{tot}/4$ with the total Frank loop

Table 3
Frank loop systems. Plane(p) denotes the normal to the plane of system p .

p	1	2	3	4
plane(p)	(111)	($\bar{1}\bar{1}1$)	($\bar{1}11$)	($\bar{1}\bar{1}1$)

Table 4
Crystal orientations, number and Schmid factor of primary slip systems. Schmid factors of primary slip systems are obtained for uniaxial tension along the axis x_1 .

Name	Crystallographic orientation along $x_1–x_2–x_3$	Number of primary slip systems	Schmid factor for primary slip systems
[100]	$[100]–[010]–[001]$	8	$\frac{1}{\sqrt{6}} \approx 0.41$
[111]	$[111]–[\bar{2}11]–[0\bar{1}1]$	6	$\frac{2}{3\sqrt{6}} \approx 0.27$
$[\bar{1}25]$	$[\bar{1}25]–[1\bar{2}1]–[210]$	1	$\frac{\sqrt{6}}{5} \approx 0.49$

density being ρ_L^{tot} [69]. b_D is the norm of the Burgers vector $\frac{1}{2}a <110>$ of dislocations and b_L is the norm of the Burgers vector $\frac{1}{2}a <111>$ of Frank loops. Two cases, unirradiated (0 dpa) and irradiated (13 dpa), are taken into account in the following simulations for emphasizing effects of the post-irradiation hardening/softening behavior on void growth and coalescence. The parameters for the two cases are listed in Table 5. Results of the simulations are presented and discussed in the following.

4.1. Void-free single crystal: a reference

Simulations are first performed using a single finite element. The results will provide a reference for comparisons with the porous single crystal. Fig. 4a shows the evolution of the overall first Piola–Kirchhoff stress component \bar{S}_{11} with respect to the strain measure $\bar{F}_{11} – 1$ of the void-free single crystal (dashed lines) for the unirradiated state (0 dpa) and the irradiated state (13 dpa) for the $[100]$ orientation at $T = 1$. Recall that the first Piola–Kirchhoff stress corresponds to the engineering stress in uniaxial tension. The strain measure $\bar{F}_{11} – 1$ corresponds the engineering strain along the principal loading direction. For 0 dpa, a strain hardening regime can be observed, which is related to the interaction among dislocations considered in eq. (24) and eq. (25). With increasing strain, \bar{S}_{11} decreases slightly, since \bar{S}_{11} is evaluated on the undeformed section. This corresponds to the cross section areal reduction of the unit cell due to finite strains. Note that the Cauchy stress $\bar{\sigma}_{11}$ is increasing in that case due to hardening and to the absence of damage. Compared to the behavior at 0 dpa, the void-free single crystal at 13 dpa displays a marked increase of the yield stress and a sharp softening at the beginning of the plastic regime followed by a slight hardening. This sharp softening corresponds, according to the observation in the experiments [2,3], to the unpinning term in eq. (24). In Fig. 4b, stress–strain curves are presented for $T = 3$. The maximum stresses at $T = 3$ are larger than those at $T = 1$. In the case of void-free crystals, the increase in stress when stress triaxiality is increased is entirely due to the pressure change for a given crystal orientation as the cell is pressure insensitive (Schmid's law); indeed the inherent plastic anisotropy plays a role when orientation is also changed.

The stress–strain curves are also shown in Fig. 5 for the $[111]$ orientation and Fig. 6 for $[\bar{1}25]$. The $[111]$ orientation exhibits similar stress–strain response as the $[100]$ orientation. A higher stress level is reached due to the lower Schmid factor of primary slip systems (see Table 4). However, the $[\bar{1}25]$ orientation displays a different response. Recall that the $[\bar{1}25]$ orientation has only one primary slip system ($s = 1$) and one secondary slip system ($s = 12$). For 0 dpa, a change in the hardening rate can be observed, which is

Table 5
Material parameters for the simulations [47,48].

C_{11}	C_{12}	C_{44}	n	τ_{ref}	$\dot{\gamma}_{\text{ref}}$
199 GPa	136 GPa	105 GPa	15	6.3 MPa	10^{-3}s^{-1}
τ_T^s	μ	g_c	κ	b_D	b_L
88 MPa	66 GPa	2.64 nm	42.8	2.54 Å	2.08 Å
a_1	a_2	a_3	a_4	a_5	a_6
0.124	0.124	0.07	0.625	0.137	0.122
b_1	b_2	b_3	b_4	b_5	b_6
0	1	1	1	1	1
0 dpa		13 dpa			
ϕ_L	—	7.3 nm			
α_L	—	0.57			
k_{dl}	—	1.7×10^{-7}			
A	—	$1.25 \times 10^{-12}\text{m}^2$			
ρ_L^{sat}	—	10^{22}m^{-3}			
τ_a	—	61.2 MPa			
γ_0	—	5×10^{-3}			
ρ_D^{ini}	—	$8.3 \times 10^8\text{m}^{-2}$	$1.6 \times 10^8\text{m}^{-2}$		
ρ_L^{ini}	—	—	$1.6 \times 10^{22}\text{m}^{-3}$		

associated with the activation of the secondary slip system leading to greater strain hardening. At 13 dpa and before the activation of the second slip system, results show the initial load drop (unpinning term) followed a limited hardening. The activation of the secondary system at about $\bar{F}_{11} - 1 = 0.25$ has several consequences: (1) it activates the unpinning term of eq. (24) for $s = 12$, as γ^{12} starts to increase, causing a dramatic drop in its slip resistance (indicated by an arrow in Fig. 8b); (2) it annihilates Frank loops in the slip plane $p = 4$, resulting in a decrease in the Frank loop density ρ_D^A (see Fig. 7b); (3) the decreasing Frank loop density leads to a small reduction in the component of the athermal slip resistance related with the dislocation-loop interaction, i.e., loop term in eq. (24), for the slip system $s = 1$ and $s = 12$ (see the blue lines in Fig. 8a and b). After this transient evolution, a smooth load decrease is once again observed due to cross section reduction.

4.2. Porous single crystal: stress–strain response

Fig. 4a also presents overall stress–strain responses of the voided single crystal (solid lines) for the [100] orientation at $T = 1$. For the voided single crystal, the stress level that can be reached is reduced compared to the void-free one at both 0 dpa and 13 dpa.

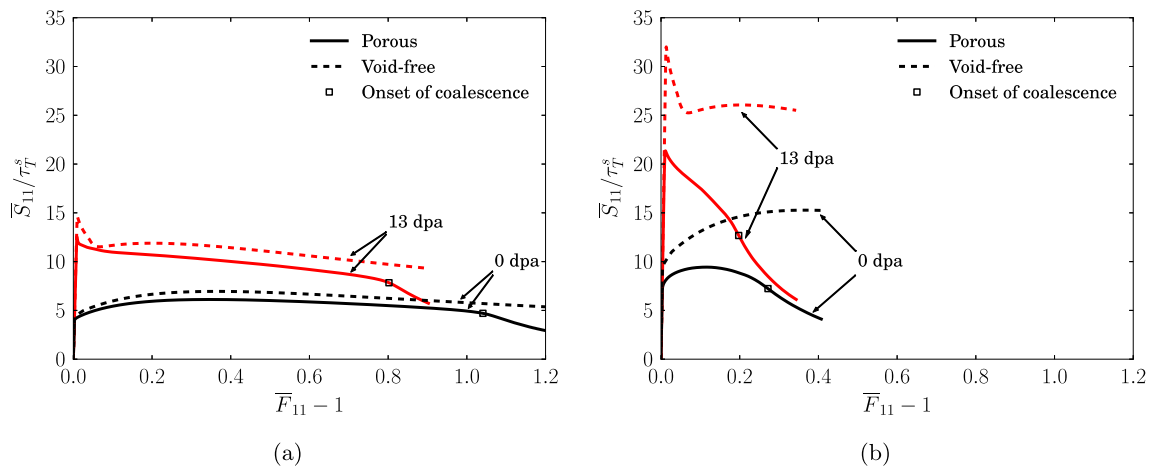


Fig. 4. Overall stress–strain curves of unit cells with void ($f_0 = 0.01$, solid lines) and without void (dashed lines) at irradiated and unirradiated state. The crystallographic orientation is [100]–[010]–[001]. (a) $T = 1$, (b) $T = 3$.

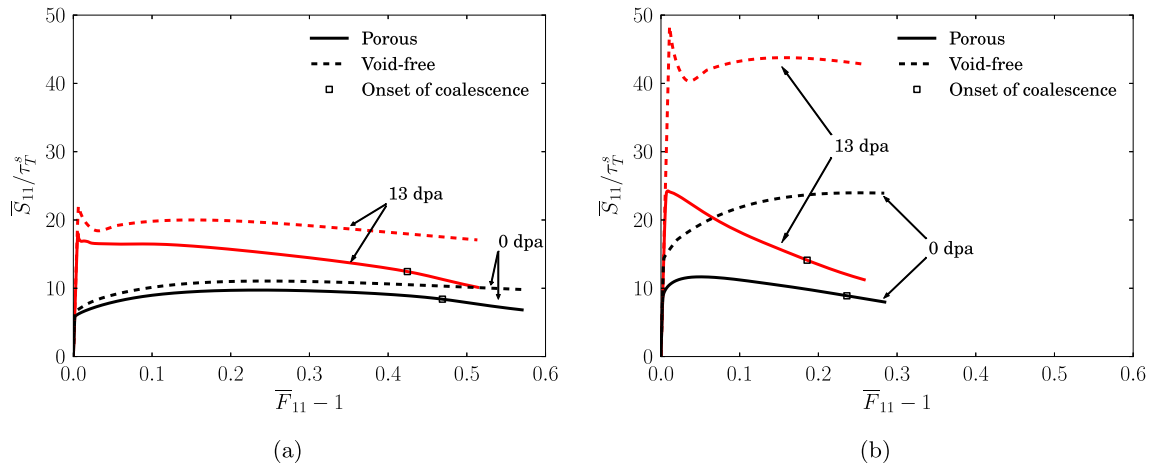


Fig. 5. Overall stress–strain curves of unit cells with void ($f_0 = 0.01$, solid lines) and without void (dashed lines) at irradiated and unirradiated state. The crystallographic orientation is [111]–[̄211]–[0̄1̄1]. (a) $T = 1$, (b) $T = 3$.

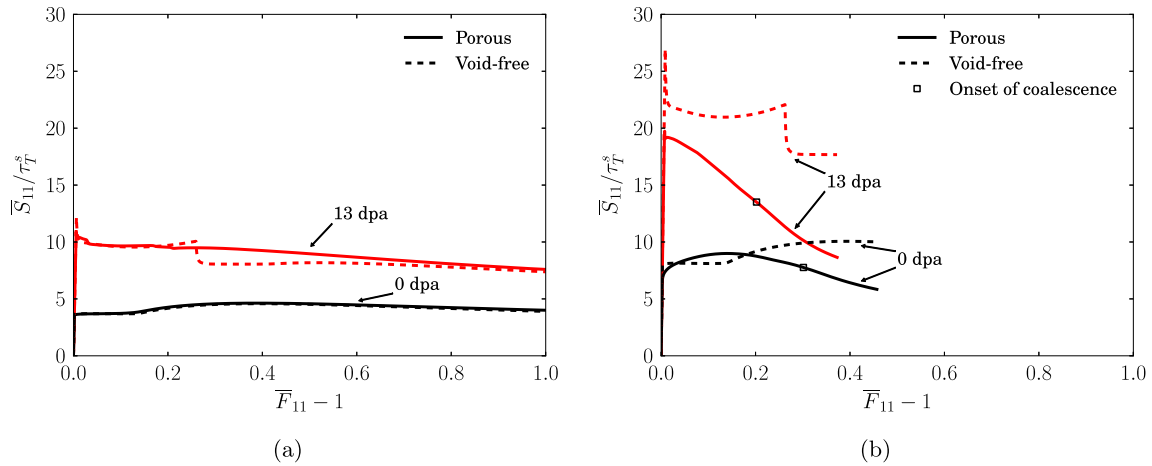


Fig. 6. Overall stress–strain curves of unit cells with void ($f_0 = 0.01$, solid lines) and without void (dashed lines) at irradiated and unirradiated state. The crystallographic orientation is $[\bar{1}25]-[\bar{1}\bar{2}1]-[210]$. (a) $T = 1$, (b) $T = 3$.

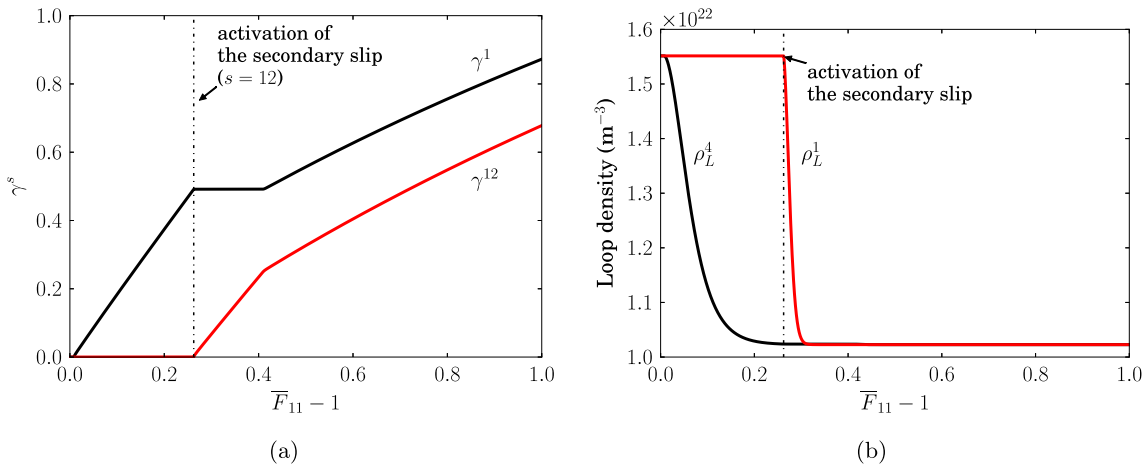


Fig. 7. Evolution of (a) plastic slip and (b) Frank loop density for the activated systems in irradiated void-free single crystal for $[\bar{1}25]$ at $T = 3$.

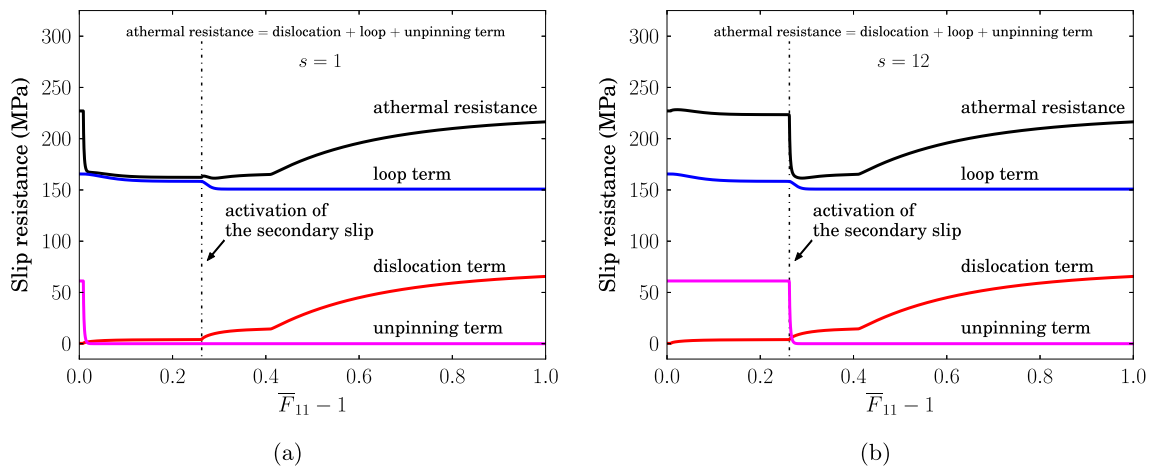


Fig. 8. Evolution of the athermal slip resistance τ_A^s and its components for the activated systems (a) $s = 1$ and (b) $s = 12$ in irradiated void-free single crystal for $[\bar{1}25]$ at $T = 3$.

Moreover, strain hardening at 0 dpa is weakened and the strain softening at 13 dpa is enhanced because of void growth. After reaching a certain strain level, the stress decreases more rapidly due to void coalescence with a greater void growth rate. This trend

is in agreement with the work of Koplik and Needleman [71] on a von Mises material. However in the present case the load drop appears as less pronounced than in this work. The onset of void coalescence (\square on the graphs) is characterized by the transition to

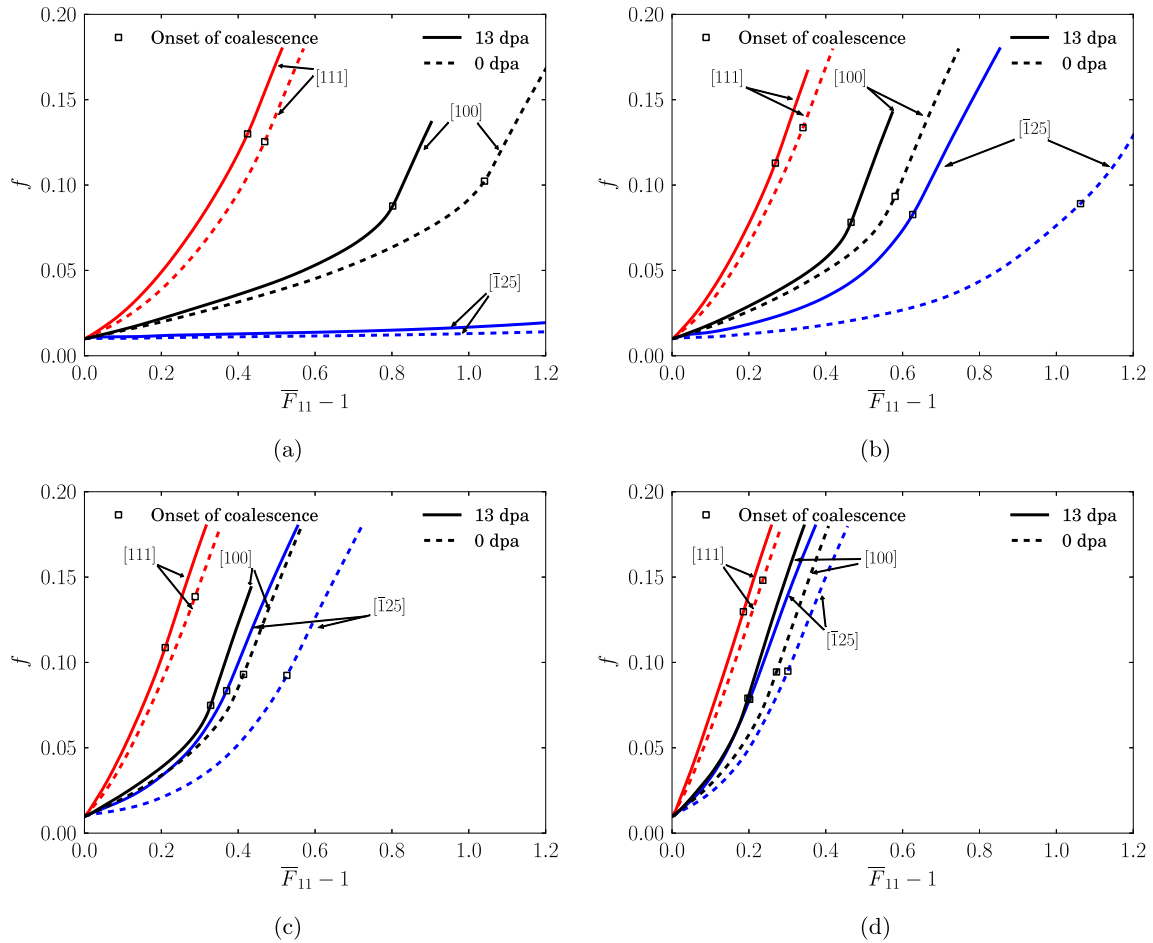


Fig. 9. Evolution of void volume fraction for three crystallographic orientations under four stress triaxialities: (a) $T = 1.0$, (b) $T = 1.5$, (c) $T = 2.0$ and (d) $T = 3.0$. $f_0 = 0.01$. Solid lines are for irradiated materials and dashed lines for unirradiated materials.

a uniaxial straining associated to the localization of the plastic flow in the intervoid ligament.

With stress triaxiality increasing up to $T = 3$ as shown in Fig. 4b, strain softening begins earlier than at $T = 1$. Voids also lead to the decrease of the yield stress. This effect is stronger for the irradiated material. The presence of the void induces a plastic strain gradient

so that the cell is progressively yielded, which prevents the macroscopic sharp peak load associated with the unpinning term. In addition, the strain hardening regime following initial softening which was observed on the void-free material completely disappears. Instead, the voided single crystal exhibits a strong softening. At the structural level this kind of behavior can lead to strain

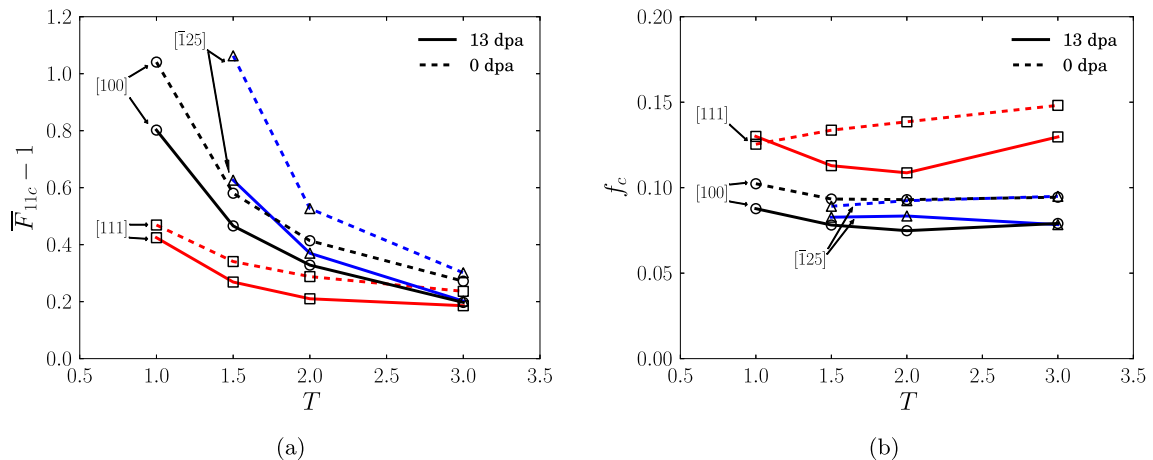


Fig. 10. Influence of stress triaxiality and crystallographic orientation on (a) the critical deformation $\bar{F}_{11c} - 1$ and (b) the critical void volume fraction f_c at the onset of coalescence for various crystallographic orientations. $f_0 = 0.01$. Solid lines are for irradiated materials and dashed lines for unirradiated materials.

localization (so called “shear bands”) and consequently to a quasi-brittle behavior.

The stress–strains curves are also shown in Fig. 5 for the [111] orientation and Fig. 6 for $\bar{1}\bar{1}2\bar{5}$. Effects of the voids shown at 0 dpa and 13 dpa for both orientations are similar to those for [100]. However some differences were observed and are described in the following. In that case the onset of coalescence does not lead to a significant change in the softening rate.

For [111], the peak stress drops by about 50% at 13 dpa at $T = 3$ due to the presence of voids. This peak drop is more severe than that observed for [100] and $\bar{1}\bar{1}2\bar{5}$. This effect is related to the low Schmid factor of this orientation. As already outlined above, the presence of voids creates a plastic strain gradient so that the local Schmid factor in areas close to the void boundary is higher than the nominal Schmid factor; this promotes an early yielding of the cell.

The presence of the plastic strain gradient around the void strongly influences the cell behavior for the $\bar{1}\bar{1}2\bar{5}$ orientation. In the voided single crystal, different slip systems are activated in the vicinity of the void and multiple slip occurs whereas single slip prevails in the sound material. As a result, the single to double slip transition is not observed. In addition, latent hardening is locally triggered at the early stages of deformation so that the voided crystal may exhibit a higher flow stress up to a given strain where void growth will induce softening (see Fig. 6b for 0 dpa).

4.3. Porous single crystal: void growth

The evolution of the void volume fraction f under a fixed stress triaxiality $T \in \{1, 1.5, 2, 3\}$ is presented in Fig. 9. As expected, void growth rate increases with the stress triaxiality for whatever orientation. For both unirradiated and irradiated single crystals, the void growth rate is the highest for the [111] orientation for all considered triaxialities and a quasi-absence of void growth is predicted for $\bar{1}\bar{1}2\bar{5}$ with $T = 1$. As shown in Ref. [16], this is due to single slip which cannot lead to void growth. For the $\bar{1}\bar{1}2\bar{5}$ orientation, however, void growth becomes significant and cannot be neglected as the stress triaxiality reaches $T = 1.5$ as shown in Fig. 9b.

Compared with unirradiated single crystal, a higher growth rate (with respect to the overall strain \bar{F}_{11}) is systematically observed in the irradiated crystal before the onset of coalescence for all investigated orientations and triaxialities. The effect of the irradiation is particularly strong at moderate stress triaxialities (i.e. $T = 1.5$ (see Fig. 9b) and $T = 2$ (see Fig. 9c)) for the $\bar{1}\bar{1}2\bar{5}$ orientation. In those cases, the void growth rate at the beginning of plastic regime is multiplied by 2.5 and 1.7 for the irradiated crystal.

4.4. Porous single crystal: onset of coalescence

According to Koplik and Needleman [71], the onset of void coalescence is characterized by the transition to a uniaxial straining associated to the localization of the plastic flow in the intervoid ligament. In this work, it is determined by plotting the transverse macroscopic strain $\bar{F}_{33} - 1$ as a function of the longitudinal macroscopic strain $\bar{F}_{11} - 1$. It is observed that $\bar{F}_{33} - 1$ reaches a stabilized value. The time step for which the transverse strain $\bar{F}_{33} - 1$ reaches 99% of its stabilized value, is regarded as the onset of coalescence. The corresponding longitudinal $\bar{F}_{11} - 1$ and porosity are defined as the critical strain $\bar{F}_{11c} - 1$ and critical porosity f_c at the onset of coalescence. Porosity f is computed as the ratio of the void volume to the cell volume. In the void coalescence regime, the void growth rate is fully determined by the coalescence kinematics (uniaxial straining).

The critical strain $\bar{F}_{11c} - 1$ for the onset of coalescence is plotted as a function of stress triaxiality T for the three orientations in

Fig. 10a. The decrease of $\bar{F}_{11c} - 1$ with increasing stress triaxiality can be observed for a given orientation. In contrast to the unirradiated cases, the onset of coalescence occurs at a smaller strain in the irradiated single crystals. Especially for the $\bar{1}\bar{1}2\bar{5}$ orientation, the decrease of $\bar{F}_{11c} - 1$ even reaches about 40% at $T = 1.5$.

The evolution of critical void volume fraction f_c for the onset of coalescence as a function of stress triaxiality T is presented in Fig. 10b. Considering one crystallographic orientation, f_c is almost unchanged for a given irradiation level. The [111] orientation shows a higher f_c than the [100] and $\bar{1}\bar{1}2\bar{5}$ orientations. With stress triaxialities varying from 1.5 to 3, similar values of f_c are predicted for [100] and $\bar{1}\bar{1}2\bar{5}$. Given one orientation, the value of f_c of the irradiated single crystals is lower than that of unirradiated ones.

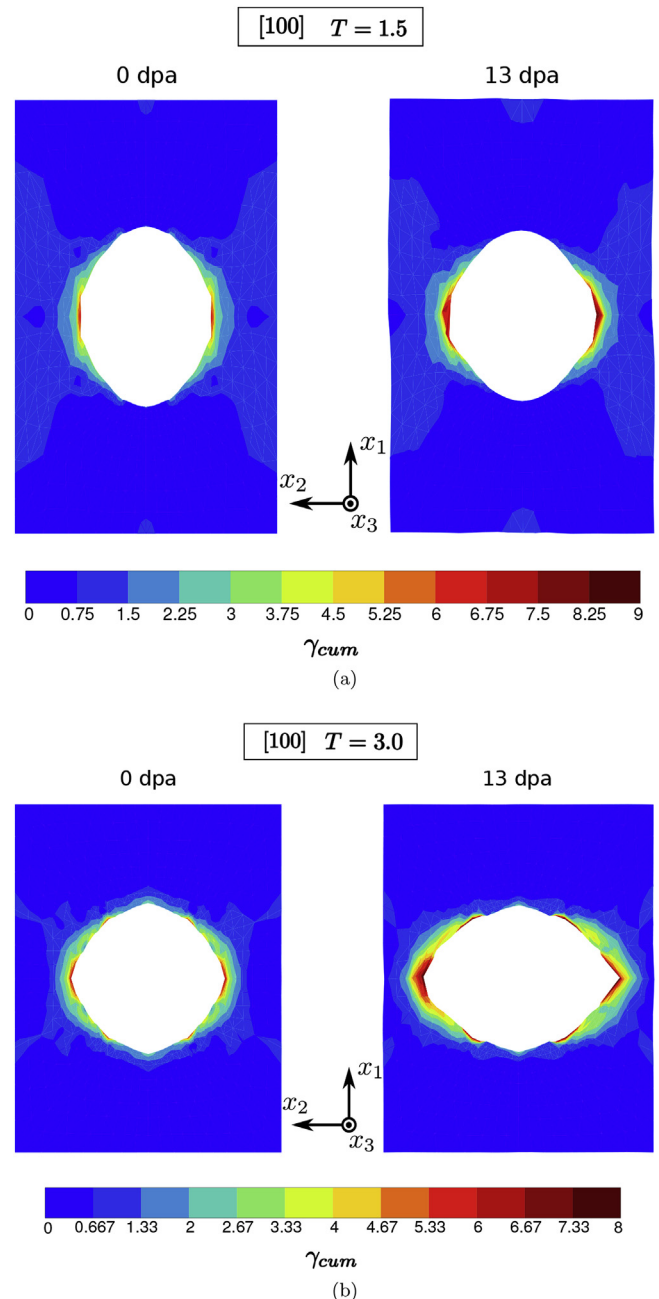


Fig. 11. Field of accumulated slip on x_1 - x_2 middle cross section on of the unit cell for [100]. (a) $T = 1.5$ and $\bar{F}_{11} - 1 = 0.35$, (b) $T = 3.0$ and $\bar{F}_{11} - 1 = 0.2$.

4.5. Porous single crystal: fields of accumulated plastic slip

In order to study the plastic deformation in the region near the void, the accumulated plastic slip γ_{cum} is considered. It is defined as:

$$\gamma_{cum} = \sum_{s=1}^{12} \gamma^s. \tag{30}$$

The fields of γ_{cum} in the middle x_1 - x_2 cross section (Fig. 2a) are shown in Fig. 11 for [100] with $T = 1.5$ ($\bar{F}_{11} - 1 = 0.35$) and $T = 3$ ($\bar{F}_{11} - 1 = 0.2$). The evolution of the void shape is different at different stress triaxialities. In particular, at a relatively low stress triaxiality $T = 1.5$, the void becomes elongated along the loading axis x_1 . Moreover, at the same stress triaxiality, a more significant localization of plastic slip is observed in the irradiated case than that in the unirradiated case, especially in the horizontal region near the void. This leads to a larger deformation of the void along the horizontal axis in the irradiated case, resulting in a faster void growth and an earlier void coalescence as shown in the previous

section (see Fig. 9). These results for the irradiated porous single crystal, combined with the rather brittle overall behavior shown in section 4.2, are consistent with Neustroev and Garner's experimental observation [11] in AISI 321 stainless steels irradiated in BOR-60, which showed an embrittlement after irradiation at the macroscopic level but a large amount of deformation at the failure site showing fine dimples.

The fields of γ_{cum} are presented for [111] and $[\bar{1}25]$ in Figs. 12 and 13. For these two orientations, the voids develop different deformed shapes. Especially for [111], a rotation of the void is observed which is caused by the shearing of the matrix, associated with the anisotropy of the single crystal. Besides, the void displays different shapes in other cross sections, e.g., the x_1 - x_3 cross section, which has been discussed in Ref. [16]; this point is out of the scope

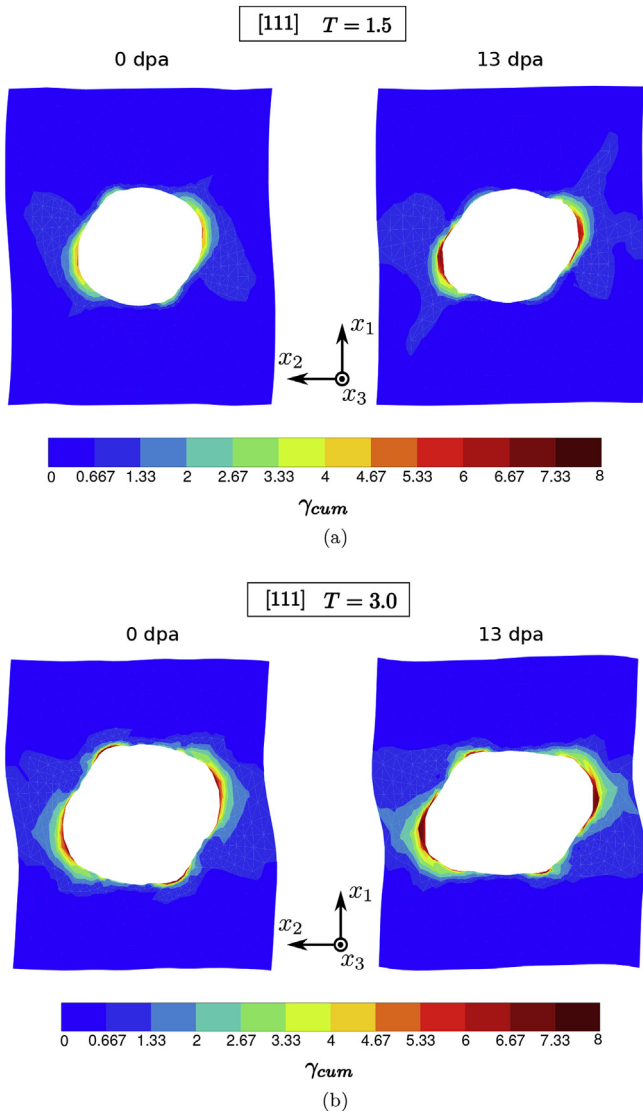


Fig. 12. Field of accumulated slip on x_1 - x_2 middle cross section on of the unit cell for [111] with (a) $T = 1.5$ and (b) $T = 3.0$. $\bar{F}_{11} - 1 = 0.14$.

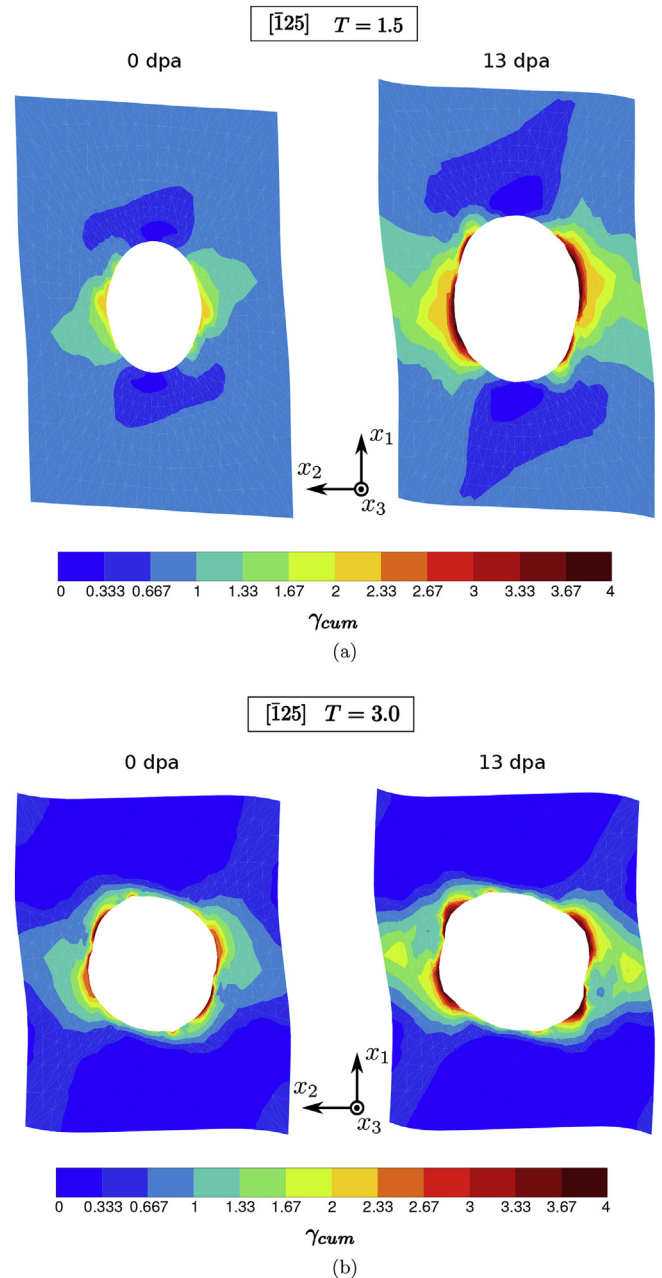


Fig. 13. Field of accumulative slip on x_1 - x_2 middle cross section of the unit cell for $[\bar{1}25]$. (a) $T = 1.5$ and $\bar{F}_{11} - 1 = 0.50$, (b) $T = 3.0$ and $\bar{F}_{11} - 1 = 0.2$.

of this work. Furthermore, in the irradiated case, again, more significant plastic slip localization can be seen for $[111]$ and $[\bar{1}25]$ than that in the unirradiated cases. Larger voids can be observed in the irradiated cases, especially for $[125]$ at $T = 1.5$ (Fig. 13a) which is consistent with faster void growth presented in Fig. 9.

Comparison of cell simulations for the un-irradiated and irradiated single crystals shows that the strong softening caused by dislocation unpinning has also no impact on the behavior of the voided cell. As mentioned above, the sharp load drop obtained for the sound single crystal disappears due to strain gradients around the void. In addition un-pinning does not cause localized deformation bands within the matrix as in the case of amorphous polymers as shown by unit cell simulations reported in Ref. [18]. This is due to the fact that softening for the single crystal occurs over a small strain increment ($< 1\%$); softening is then immediately followed by hardening. Due to the strain gradient a localized band cannot be formed. The situation is opposite in the case of polymers as softening is observed over wide plastic strain ranges (up to 50%).

5. Conclusions

In this work, the void growth and coalescence at constant stress triaxiality in irradiated FCC single crystals are investigated using unit cell FE simulations. A single crystal plasticity model is used accounting for the modification of mechanical properties associated to the irradiation-induced defects. From these unit cell simulations, the following conclusions can be drawn:

- The crystal orientation, i.e., the plastic anisotropy, has a significant impact on void growth in FCC single crystals, which has already been shown in a previous work [16].
- Voids grow at a higher rate in the irradiated single crystal in relation with a lower hardening rate as observed for von Mises matrix materials [72].
- The onset of void coalescence occurs at a smaller value of the overall strain and at a smaller value of the void volume fraction in the irradiated crystals.
- More significant plastic strain localization in the region near the void is predicted in the irradiated crystal, correlated with the faster void growth and earlier onset of void coalescence.

- Brittle-like overall behavior is predicted at high level of stress triaxiality, i.e. $T = 3$, in the voided irradiated crystal, while a large amount of plastic deformation is reached in the vicinity of the void. These results are in agreement with the experimental observations in the literature.
- For a given crystal orientation, the porosity at coalescence does not depend on stress triaxiality. However the corresponding value depends on crystal orientation.

It should be noted that the interaction between channel deformation and void growth which has been observed in Ref. [8] is not considered in the present work. According to [8], channel deformation can decrease void growth rate. In addition to unit cell simulations, the effective behaviors of voided single crystals have been modeled in Ref. [16] at finite strains and the model can be extended by coupling it with the crystal plasticity model for irradiated materials presented in this work.

In addition, intragranular voids have considered in this work; they can correspond to irradiation-induced swelling voids or to voids nucleated on irradiation-induced precipitates during plastic straining. The former can lead to nano-sized fracture dimples and their size can be as small as 20–30 nm according to [8]. The latter, as reported in Ref. [9], can result in fracture dimples of size $< 10 \mu\text{m}$ in irradiated steels, which is smaller than in unirradiated materials size $> 25 \mu\text{m}$. In a word, voids of different sizes exist in irradiated steels. Moreover, it is well known that size effects in plasticity exist at the crystal level (see, e.g., [73–77]) and size effects in turn are also expected on void growth and coalescence [78,79]. It is hence of importance to investigate the effect of void size on the ductile fracture process and fracture toughness at the grain scale. This can be done using enhanced continuum theories for the single crystal accounting for internal lengths such as those in Refs. [80–82]. This aspect will be considered in a future work.

Appendix A. Form of the a^{su} and b^{su} matrices

In FCC single crystals, the matrices a^{su} and b^{su} ($s, u = 1, 2, \dots, 12$) have respectively $12 \times 12 = 144$ coefficients. For symmetry reasons, the number of coefficients is reduced to six, i.e., a_i and b_i with $i = 1, 2, \dots, 6$ [83]. a^{su} is constructed as follows:

$$[a^{su}] = \begin{matrix} & \begin{matrix} A2 & A3 & A6 & B2 & B4 & B5 & C1 & C3 & C5 & D1 & D4 & D6 \end{matrix} \\ \begin{matrix} a1 & a2 & a2 & a4 & a5 & a5 & a3 & a5 & a6 & a3 & a6 & a5 \end{matrix} & \begin{matrix} A2 \\ A3 \\ A6 \\ B2 \\ B4 \\ B5 \\ C1 \\ C3 \\ C5 \\ D1 \\ D4 \\ D6 \end{matrix} \\ \begin{matrix} & a1 & a2 & a5 & a3 & a6 & a5 & a4 & a5 & a6 & a3 & a5 \end{matrix} & \begin{matrix} A3 \\ A6 \\ B2 \\ B4 \\ B5 \\ C1 \\ C3 \\ C5 \\ D1 \\ D4 \\ D6 \end{matrix} \\ \begin{matrix} & & a1 & a5 & a6 & a3 & a6 & a5 & a3 & a5 & a5 & a4 \end{matrix} & \begin{matrix} A6 \\ B2 \\ B4 \\ B5 \\ C1 \\ C3 \\ C5 \\ D1 \\ D4 \\ D6 \end{matrix} \\ \begin{matrix} & & & a1 & a2 & a2 & a3 & a6 & a5 & a3 & a5 & a6 \end{matrix} & \begin{matrix} B2 \\ B4 \\ B5 \\ C1 \\ C3 \\ C5 \\ D1 \\ D4 \\ D6 \end{matrix} \\ \begin{matrix} & & & & a1 & a2 & a6 & a3 & a5 & a5 & a4 & a5 \end{matrix} & \begin{matrix} B4 \\ B5 \\ C1 \\ C3 \\ C5 \\ D1 \\ D4 \\ D6 \end{matrix} \\ \begin{matrix} & & & & & a1 & a5 & a5 & a4 & a6 & a5 & a3 \end{matrix} & \begin{matrix} B5 \\ C1 \\ C3 \\ C5 \\ D1 \\ D4 \\ D6 \end{matrix} \\ \begin{matrix} & & & & & & a1 & a2 & a2 & a4 & a5 & a5 \end{matrix} & \begin{matrix} C1 \\ C3 \\ C5 \\ D1 \\ D4 \\ D6 \end{matrix} \\ \begin{matrix} & & & & & & & a1 & a2 & a5 & a3 & a6 \end{matrix} & \begin{matrix} C3 \\ C5 \\ D1 \\ D4 \\ D6 \end{matrix} \\ \begin{matrix} & & & & & & & & a1 & a5 & a6 & a3 \end{matrix} & \begin{matrix} C5 \\ D1 \\ D4 \\ D6 \end{matrix} \\ \begin{matrix} & & & & & & & & & a1 & a2 & a2 \end{matrix} & \begin{matrix} D1 \\ D4 \\ D6 \end{matrix} \\ \begin{matrix} & & & & & & & & & & a1 & a2 \end{matrix} & \begin{matrix} D4 \\ D6 \end{matrix} \\ \begin{matrix} & & & & & & & & & & & a1 \end{matrix} & \begin{matrix} D6 \end{matrix} \end{matrix} \quad (\text{A.1})$$

In the matrix, a_1 corresponds to self hardening, a_2 to coplanar interaction, a_3 to Hirth locks, a_4 to collinear interaction, a_5 to glissile junctions and a_6 to Lomer locks. The matrix b^{su} has the same structure as a^{su} and is not presented here for the sake of brevity.

References

- [1] J. Pawel, A. Rowcliffe, D. Alexander, M. Grossbeck, K. Shiba, Effects of low temperature neutron irradiation on deformation behavior of austenitic stainless steels, *J. Nucl. Mater.* 233 (1996) 202–206. [http://dx.doi.org/10.1016/S0022-3115\(96\)00218-8](http://dx.doi.org/10.1016/S0022-3115(96)00218-8). <http://www.sciencedirect.com/science/article/pii/S0022311596002188>.
- [2] C. Pokor, X. Averty, Y. Bréchet, P. Dubuisson, J. Massoud, Effect of irradiation defects on the work hardening behavior, *Scr. Mater.* 50 (5) (2004) 597–600. <http://dx.doi.org/10.1016/j.scriptamat.2003.11.029>. <http://www.sciencedirect.com/science/article/pii/S1359646203007590>.
- [3] C. Pokor, Y. Bréchet, P. Dubuisson, J.-P. Massoud, X. Averty, Irradiation damage in 304 and 316 stainless steels: experimental investigation and modeling. Part II: irradiation induced hardening, *J. Nucl. Mater.* 326 (1) (2004) 30–37. <http://dx.doi.org/10.1016/j.jnucmat.2003.12.008>. <http://www.sciencedirect.com/science/article/pii/S0022311503005361>.
- [4] C. Pokor, Y. Bréchet, P. Dubuisson, J.-P. Massoud, A. Barbu, Irradiation damage in 304 and 316 stainless steels: experimental investigation and modeling. Part I: evolution of the microstructure, *J. Nucl. Mater.* 326 (1) (2004) 19–29. <http://dx.doi.org/10.1016/j.jnucmat.2003.11.007>. <http://www.sciencedirect.com/science/article/pii/S0022311503005129>.
- [5] K. Fukuya, K. Fujii, H. Nishioka, Y. Kitsunai, Evolution of microstructure and microchemistry in cold-worked 316 stainless steels under PWR irradiation, *J. Nucl. Sci. Technol.* 43 (2) (2006) 159–173.
- [6] Z. Jiao, G. Was, The role of irradiated microstructure in the localized deformation of austenitic stainless steels, *J. Nucl. Mater.* 407 (1) (2010) 34–43 proceedings of the Symposium on Microstructural Processes in Irradiated Materials and on Reactor Pressure Vessel (RPV) Embrittlement and Fusion Materials: Measuring, Modeling and Managing Irradiation Effects, <http://dx.doi.org/10.1016/j.jnucmat.2010.07.006>, <http://www.sciencedirect.com/science/article/pii/S0022311510002916>.
- [7] S. Zinkle, G. Was, Materials challenges in nuclear energy, *Acta Mater.* 61 (3) (2013) 735–758 the Diamond Jubilee Issue Materials Challenges in Tomorrow's World Selected Topics in Materials Science and Engineering, <http://dx.doi.org/10.1016/j.actamat.2012.11.004>. <http://www.sciencedirect.com/science/article/pii/S1359645412007987>.
- [8] B. Margolin, A. Sorokin, V. Shvetsova, A. Minkin, V. Potapova, V. Smirnov, The radiation swelling effect on fracture properties and fracture mechanisms of irradiated austenitic steels. part i. ductility and fracture toughness, *J. Nucl. Mater.* 480 (2016) 52–68. <http://dx.doi.org/10.1016/j.jnucmat.2016.07.051>. <http://www.sciencedirect.com/science/article/pii/S002231151630472X>.
- [9] E. Little, Fracture mechanics evaluations of neutron irradiated type 321 austenitic steel, *J. Nucl. Mater.* 139 (3) (1986) 261–276. [http://dx.doi.org/10.1016/0022-3115\(86\)90179-0](http://dx.doi.org/10.1016/0022-3115(86)90179-0). <http://www.sciencedirect.com/science/article/pii/0022311586901790>.
- [10] K. Fukuya, H. Nishioka, K. Fujii, M. Kamaya, T. Miura, T. Torimaru, Fracture behavior of austenitic stainless steels irradiated in PWR, *J. Nucl. Mater.* 378 (2) (2008) 211–219. <http://dx.doi.org/10.1016/j.jnucmat.2008.06.028>. <http://www.sciencedirect.com/science/article/pii/S0022311508003553>.
- [11] V. Neustroev, F. Garner, Severe embrittlement of neutron irradiated austenitic steels arising from high void swelling, *J. Nucl. Mater.* 386388 (2009) 157–160. Fusion Reactor Materials Proceedings of the Thirteenth International Conference on Fusion Reactor Materials, <http://dx.doi.org/10.1016/j.jnucmat.2008.12.077>. <http://www.sciencedirect.com/science/article/pii/S0022311508008295>.
- [12] B. Margolin, G. Karzov, V. Shvetsova, V. Kostylev, Modelling for transcrystalline and intercrystalline fracture by void nucleation and growth, *Fatigue Fract. Eng. Mater. Struct.* 21 (2) (1998) 123–137.
- [13] B. Margolin, A. Sorokin, V. Smirnov, V. Potapova, Physical and mechanical modelling of neutron irradiation effect on ductile fracture. Part 1. Prediction of fracture strain and fracture toughness of austenitic steels, *J. Nucl. Mater.* 452 (13) (2014) 595–606. <http://dx.doi.org/10.1016/j.jnucmat.2014.03.047>. <http://www.sciencedirect.com/science/article/pii/S002231151400172X>.
- [14] B. Margolin, A. Sorokin, Physical and mechanical modeling of the neutron irradiation effect on ductile fracture. Part 2. Prediction of swelling effect on drastic decrease in strength, *J. Nucl. Mater.* 452 (13) (2014) 607–613. <http://dx.doi.org/10.1016/j.jnucmat.2014.05.050>. <http://www.sciencedirect.com/science/article/pii/S0022311514003274>.
- [15] S. Yerra, C. Tekoglu, F. Scheyvaerts, L. Delannay, P.V. Houtte, T. Pardoen, Void growth and coalescence in single crystals, *Int. J. Solids Struct.* 47 (7–8) (2010) 1016–1029. <http://dx.doi.org/10.1016/j.ijsolstr.2009.12.019>. <http://www.sciencedirect.com/science/article/pii/S0020768309004909>.
- [16] C. Ling, J. Besson, S. Forest, B. Tanguy, F. Latourte, E. Bosso, An elastoviscoplastic model for porous single crystals at finite strains and its assessment based on unit cell simulations, *Int. J. Plast.* 84 (2016) 58–87. <http://dx.doi.org/10.1016/j.iplas.2016.05.001>. <http://www.sciencedirect.com/science/article/pii/S0749641916300699>.
- [17] A. Steenbrink, E.V.D. Giessen, P. Wu, Void growth in glassy polymers, *J. Mech. Phys. Solids* 45 (3) (1997) 405–437. [http://dx.doi.org/10.1016/S0022-5096\(96\)00093-2](http://dx.doi.org/10.1016/S0022-5096(96)00093-2). <http://www.sciencedirect.com/science/article/pii/S0022509696000932>.
- [18] A.C. Steenbrink, E. Van Der Giessen, P.D. Wu, Studies on the growth of voids in amorphous glassy polymers, *J. Mater. Sci.* 33 (12) (1998) 3163–3175. <http://dx.doi.org/10.1023/A:1004356108870>. <http://dx.doi.org/10.1023/A:1004356108870>.
- [19] M. Danielsson, D. Parks, M. Boyce, Three-dimensional micromechanical modeling of voided polymeric materials, *J. Mech. Phys. Solids* 50 (2) (2002) 351–379. [http://dx.doi.org/10.1016/S0022-5096\(01\)00060-6](http://dx.doi.org/10.1016/S0022-5096(01)00060-6). <http://www.sciencedirect.com/science/article/pii/S0022509601000606>.
- [20] M. Danielsson, D.M. Parks, M.C. Boyce, Micromechanics, macromechanics and constitutive modeling of the elasto-viscoplastic deformation of rubber-toughened glassy polymers, *J. Mech. Phys. Solids* 55 (3) (2007) 533–561. <http://dx.doi.org/10.1016/j.jmps.2006.08.006>. <http://www.sciencedirect.com/science/article/pii/S0022509606001347>.
- [21] F.A. McClintock, A criterion for ductile fracture by the growth of holes, *J. Appl. Mech.* 35 (2) (1968) 363–371.
- [22] J. Rice, D. Tracey, On the ductile enlargement of voids in triaxial stress fields, *J. Mech. Phys. Solids* 17 (3) (1969) 201–217. [http://dx.doi.org/10.1016/0022-5096\(69\)90033-7](http://dx.doi.org/10.1016/0022-5096(69)90033-7). <http://www.sciencedirect.com/science/article/pii/0022509669900337>.
- [23] A.L. Gurson, Continuum theory of ductile rupture by void nucleation and growth: Part I—yield criteria and flow rules for porous ductile media, *J. Eng. Mater. Technol.* 99 (1) (1977) 2–15.
- [24] J. Besson, Continuum models of ductile fracture: a review, *Int. J. Damage Mech.* 19 (1) (2010) 3–52. <http://dx.doi.org/10.1177/1056789509103482> arXiv:<http://ijd.sagepub.com/content/19/1/3.full.pdf+html>, <http://ijd.sagepub.com/content/19/1/3.abstract>.
- [25] A. Benzerga, J.-B. Leblond, Ductile fracture by void growth to coalescence, *Adv. Appl. Mech.* 44 (2010) 169–305.
- [26] A. Pineau, A. Benzerga, T. Pardoen, Failure of metals I: brittle and ductile fracture, *Acta Mater.* 107 (2016) 424–483. <http://dx.doi.org/10.1016/j.actamat.2015.12.034>. <http://www.sciencedirect.com/science/article/pii/S1359645415301403>.
- [27] A. Needleman, Void growth in an elastic-plastic medium, *J. Appl. Mech.* 39 (4) (1972) 964–970.
- [28] A. Needleman, A continuum model for void nucleation by inclusion debonding, *J. Appl. Mech.* 54 (3) (1987) 525–531.
- [29] D. Steglich, W. Brocks, Selected papers of the sixth international workshop on computational mechanics of materials micromechanical modelling of the behaviour of ductile materials including particles, *Comput. Mater. Sci.* 9 (1) (1997) 7–17. [http://dx.doi.org/10.1016/S0927-0256\(97\)00053-0](http://dx.doi.org/10.1016/S0927-0256(97)00053-0). <http://www.sciencedirect.com/science/article/pii/S0927025697000530>.
- [30] J. Koplik, A. Needleman, Void growth and coalescence in porous plastic solids, *Int. J. Solids Struct.* 24 (8) (1988) 835–853. [http://dx.doi.org/10.1016/0020-7683\(88\)90051-0](http://dx.doi.org/10.1016/0020-7683(88)90051-0). <http://www.sciencedirect.com/science/article/pii/0020768388900510>.
- [31] M. Worswick, R. Pick, Void growth and constitutive softening in a periodically voided solid, *J. Mech. Phys. Solids* 38 (5) (1990) 601–625. [http://dx.doi.org/10.1016/0022-5096\(90\)90025-Y](http://dx.doi.org/10.1016/0022-5096(90)90025-Y). <http://www.sciencedirect.com/science/article/pii/002250969090025Y>.
- [32] T. Pardoen, J. Hutchinson, An extended model for void growth and coalescence, *J. Mech. Phys. Solids* 48 (12) (2000) 2467–2512. [http://dx.doi.org/10.1016/S0022-5096\(00\)00019-3](http://dx.doi.org/10.1016/S0022-5096(00)00019-3). <http://www.sciencedirect.com/science/article/pii/S0022509600000193>.
- [33] A.A. Benzerga, J. Besson, Plastic potentials for anisotropic porous solids, *Eur. J. Mech. - A/Solids* 20 (3) (2001) 397–434. [http://dx.doi.org/10.1016/S0997-7538\(01\)01147-0](http://dx.doi.org/10.1016/S0997-7538(01)01147-0). <http://www.sciencedirect.com/science/article/pii/S0997753801011470>.
- [34] Zset. <http://www.zset-software.com>.
- [35] J. Besson, R. Foerch, Object-oriented programming applied to the finite element method part I. general concepts, *Rev. Eur. Des. Éléments Finis* 7 (5) (1998) 535–566. <http://dx.doi.org/10.1080/12506559.1998.10511321>. <http://www.tandfonline.com/doi/abs/10.1080/12506559.1998.10511321>.
- [36] X. Han, J. Besson, S. Forest, B. Tanguy, S. Bugat, A yield function for single crystals containing voids, *Int. J. Solids Struct.* 50 (2013) 2115–2131.
- [37] A.S. Kalchenko, V.V. Bryk, N.P. Lazarev, V.N. Voyevodin, F.A. Garner, Prediction of void swelling in the baffle ring of WWER-1000 reactors for service life of 30–60 years, *J. Nucl. Mater.* 437 (1–3) (2013) 415–423. <http://dx.doi.org/10.1016/j.jnucmat.2013.02.010>.
- [38] X. Xiao, D. Terentyev, L. Yu, A. Bakaev, Z. Jin, H. Duan, Investigation of the thermo-mechanical behavior of neutron-irradiated Fe-Cr alloys by self-consistent plasticity theory, *J. Nucl. Mater.* 477 (2016) 123–133. <http://dx.doi.org/10.1016/j.jnucmat.2016.05.012>. <http://www.sciencedirect.com/science/article/pii/S0022311516301933>.
- [39] N.R. Barton, A. Arsenlis, J. Marian, A polycrystal plasticity model of strain localization in irradiated iron, *J. Mech. Phys. Solids* 61 (2) (2013) 341–351. <http://dx.doi.org/10.1016/j.jmps.2012.10.009>. <http://www.sciencedirect.com/science/article/pii/S002250961200230X>.
- [40] X. Hu, D. Xu, T.S. Byun, B.D. Wirth, Modeling of irradiation hardening of iron after low-dose and low-temperature neutron irradiation, *Model. Simul. Mater. Sci. Eng.* 22 (6) (2014), 065002. <http://stacks.iop.org/0965-0393/22/i=6>

- a=065002.
- [41] X. Xiao, D. Terentyev, L. Yu, D. Song, A. Bakaev, H. Duan, Modelling irradiation-induced softening in BCC iron by crystal plasticity approach, *J. Nucl. Mater.* 466 (2015) 312–315. <http://dx.doi.org/10.1016/j.jnucmat.2015.08.017>. <http://www.sciencedirect.com/science/article/pii/S0022311515301562>.
- [42] A. Arsenlis, B.D. Wirth, M. Rhee, Dislocation density-based constitutive model for the mechanical behaviour of irradiated Cu, *Philos. Mag.* 84 (34) (2004) 3617–3635. <http://dx.doi.org/10.1080/14786430412331293531>. <http://dx.doi.org/10.1080/14786430412331293531>.
- [43] Rahul S. De, Multiscale modeling of irradiated polycrystalline FCC metals, *Int. J. Solids Struct.* 51 (2324) (2014) 3919–3930. <http://dx.doi.org/10.1016/j.ijsolstr.2014.07.015>. <http://www.sciencedirect.com/science/article/pii/S0020768314002893>.
- [44] X. Xiao, D. Song, J. Xue, H. Chu, H. Duan, A self-consistent plasticity theory for modeling the thermo-mechanical properties of irradiated FCC metallic polycrystals, *J. Mech. Phys. Solids* 78 (2015) 1–16. <http://dx.doi.org/10.1016/j.jmps.2015.01.011>. <http://www.sciencedirect.com/science/article/pii/S0022509615000204>.
- [45] A. Patra, D.L. McDowell, Crystal plasticity-based constitutive modelling of irradiated bcc structures, *Philos. Mag.* 92 (7) (2012) 861–887. <http://dx.doi.org/10.1080/14786435.2011.634855>. <http://dx.doi.org/10.1080/14786435.2011.634855>.
- [46] A. Patra, D.L. McDowell, Continuum modeling of localized deformation in irradiated bcc materials, *J. Nucl. Mater.* 432 (13) (2013) 414–427. <http://dx.doi.org/10.1016/j.jnucmat.2012.08.021>. <http://www.sciencedirect.com/science/article/pii/S0022311512004308>.
- [47] X. Han, Modélisation de la fragilisation due au gonflement dans les aciers inoxydables austénitiques irradiés, Ph.D. thesis, Mines ParisTech, 2012.
- [48] J. Hure, S.E. Shawish, L. Cizelj, B. Tanguy, Intergranular stress distributions in polycrystalline aggregates of irradiated stainless steel, *J. Nucl. Mater.* 476 (2016) 231–242. <http://dx.doi.org/10.1016/j.jnucmat.2016.04.017>. <http://www.sciencedirect.com/science/article/pii/S0022311516301313>.
- [49] E.H. Lee, Elastic-plastic deformation at finite strains, *J. Appl. Mech.* 36 (1) (1969) 1–6.
- [50] J. Mandel, Equations constitutives et directeurs dans les milieux plastiques et viscoplastiques, *Int. J. Solids Struct.* 9 (6) (1973) 725–740. [http://dx.doi.org/10.1016/0020-7683\(73\)90120-0](http://dx.doi.org/10.1016/0020-7683(73)90120-0). <http://www.sciencedirect.com/science/article/pii/0020768373901200>.
- [51] P. Sabnis, M. Mazière, S. Forest, N.K. Arakere, F. Ebrahimi, Effect of secondary orientation on notch-tip plasticity in superalloy single crystals, *Int. J. Plast.* 28 (1) (2012) 102–123. <http://dx.doi.org/10.1016/j.ijplas.2011.06.003>. <http://www.sciencedirect.com/science/article/pii/S0749641911001045>.
- [52] P.A. Sabnis, S. Forest, N.K. Arakere, V.A. Yastrebov, Crystal plasticity analysis of cylindrical indentation on a Ni-base single crystal superalloy, *Int. J. Plast.* 51 (2013) 200–217. <http://dx.doi.org/10.1016/j.ijplas.2013.05.004>. <http://www.sciencedirect.com/science/article/pii/S0749641913001022>.
- [53] P. Franciosi, A. Zaoui, Multislip in f.c.c. crystals a theoretical approach compared with experimental data, *Acta Metall.* 30 (8) (1982) 1627–1637. [http://dx.doi.org/10.1016/0001-6160\(82\)90184-5](http://dx.doi.org/10.1016/0001-6160(82)90184-5). <http://www.sciencedirect.com/science/article/pii/0001616082901845>.
- [54] H. Mughrabi, *Materials Science and Technology, Plastic Deformation and Fracture of Materials*, Materials Science and Technology, Wiley, 1996.
- [55] B. Tanguy, X. Han, J. Besson, S. Forest, C. Robertson, N. Rupin, Dislocations and irradiation defects-based micromechanical modelling for neutron irradiated austenitic stainless steels, in: *International Symposium on Plasticity and its Current Applications*, 2013.
- [56] H. Trinkaus, B. Singh, A. Foreman, Mechanisms for decoration of dislocations by small dislocation loops under cascade damage conditions, *J. Nucl. Mater.* 249 (2) (1997) 91–102. [http://dx.doi.org/10.1016/S0022-3115\(97\)00230-4](http://dx.doi.org/10.1016/S0022-3115(97)00230-4). <http://www.sciencedirect.com/science/article/pii/S0022311597002304>.
- [57] H. Trinkaus, B. Singh, A. Foreman, Proceedings of the international workshop on defect production, accumulation and materials performance in an irradiation environment segregation of cascade induced interstitial loops at dislocations: possible effect on initiation of plastic deformation, *J. Nucl. Mater.* 251 (1997) 172–187. [http://dx.doi.org/10.1016/S0022-3115\(97\)00246-8](http://dx.doi.org/10.1016/S0022-3115(97)00246-8). <http://www.sciencedirect.com/science/article/pii/S0022311597002468>.
- [58] B. Singh, A. Foreman, H. Trinkaus, Radiation hardening revisited: role of intracascade clustering, *J. Nucl. Mater.* 249 (2) (1997) 103–115. [http://dx.doi.org/10.1016/S0022-3115\(97\)00231-6](http://dx.doi.org/10.1016/S0022-3115(97)00231-6). <http://www.sciencedirect.com/science/article/pii/S0022311597002316>.
- [59] H. Mecking, K. Lücke, A new aspect of the theory of flow stress of metals, *Scr. Metall.* 4 (6) (1970) 427–432. [http://dx.doi.org/10.1016/0036-9748\(70\)90078-5](http://dx.doi.org/10.1016/0036-9748(70)90078-5). <http://www.sciencedirect.com/science/article/pii/0036974870900785>.
- [60] U. Essmann, M. Rapp, Slip in copper crystals following weak neutron bombardment, *Acta Metall.* 21 (9) (1973) 1305–1317. [http://dx.doi.org/10.1016/0001-6160\(73\)90172-7](http://dx.doi.org/10.1016/0001-6160(73)90172-7). <http://www.sciencedirect.com/science/article/pii/0001616073901727>.
- [61] C. Teodosiu, P. Sidoroff, A finite theory of the elastoviscoplasticity of single crystals, *Int. J. Eng. Sci.* 14 (8) (1976) 713–723. [http://dx.doi.org/10.1016/0020-7225\(76\)90027-6](http://dx.doi.org/10.1016/0020-7225(76)90027-6). <http://www.sciencedirect.com/science/article/pii/0020722576900276>.
- [62] L. Tabourot, M. Fivel, E. Rauch, Generalised constitutive laws for f.c.c. single crystals, *Mater. Sci. Eng. A* 234 (1997) 639–642. [http://dx.doi.org/10.1016/S0921-5093\(97\)00353-5](http://dx.doi.org/10.1016/S0921-5093(97)00353-5). <http://www.sciencedirect.com/science/article/pii/S0921509397003535>.
- [63] K.-S. Cheong, E.P. Busso, Discrete dislocation density modelling of single phase {FCC} polycrystal aggregates, *Acta Mater.* 52 (19) (2004) 5665–5675. <http://dx.doi.org/10.1016/j.actamat.2004.08.044>. <http://www.sciencedirect.com/science/article/pii/S1359645404005099>.
- [64] D. Rodney, G. Martin, Dislocation pinning by small interstitial loops: a molecular dynamics study, *Phys. Rev. Lett.* 82 (1999) 3272–3275. <http://dx.doi.org/10.1103/PhysRevLett.82.3272>. <http://link.aps.org/doi/10.1103/PhysRevLett.82.3272>.
- [65] Y. Yang, H. Abe, N. Sekimura, Behavior of Frank-loops under stress environment, *Phys. Lett. A* 315 (34) (2003) 293–300. [http://dx.doi.org/10.1016/S0375-9601\(03\)01016-8](http://dx.doi.org/10.1016/S0375-9601(03)01016-8). <http://www.sciencedirect.com/science/article/pii/S0375960103010168>.
- [66] S. Krishna, A. Zamiri, S. De, Dislocation and defect density-based micro-mechanical modeling of the mechanical behavior of fcc metals under neutron irradiation, *Philos. Mag.* 90 (30) (2010) 4013–4025.
- [67] S. Krishna, S. De, A temperature and rate-dependent micromechanical model of molybdenum under neutron irradiation, *Mech. Mater.* 43 (2) (2011) 99–110. <http://dx.doi.org/10.1016/j.mechmat.2010.12.005>. <http://www.sciencedirect.com/science/article/pii/S0167663610001687>.
- [68] G. Monnet, A Crystalline Plasticity Law for Austenitic Stainless Steel, eDF R&D internal report, PERFORM Projet, H-B60-2008-04690-EN, 2009.
- [69] Alexandra Renault, Joël Malaplate, Cédric Pokor, Pierre Gavoille, Jean-Paul Massoud, Jérôme Garnier, Effects of chemical composition, metallurgical state and stress during irradiation on microstructure of neutron-irradiated austenitic stainless steels: comparison of PWR and BOR-60 irradiations, Fontevraud 7 - Contribution of materials investigations to improve the safety and performance of LWRs, Avignon, France, 2010.
- [70] V.E. Schmid, W. Boas, *Kristallplastizität*, Verlag Julius Springer, Berlin, 1935.
- [71] J. Koplik, A. Needleman, Void growth and coalescence in porous plastic solids, *Int. J. Solids Struct.* 24 (8) (1988) 835–853. [http://dx.doi.org/10.1016/0020-7683\(88\)90051-0](http://dx.doi.org/10.1016/0020-7683(88)90051-0). <http://www.sciencedirect.com/science/article/pii/0020768388900510>.
- [72] J. Faleskog, C. Shih, *Micromechanics of coalescence — I. Synergistic effects of elasticity, plastic yielding and multi-size-scale voids*, *J. Mech. Phys. Solids* 45 (1) (1997) 21–50.
- [73] N. Fleck, G. Muller, M. Ashby, J. Hutchinson, Strain gradient plasticity: theory and experiment, *Acta Metallurgica Materialia* 42 (2) (1994) 475–487. [http://dx.doi.org/10.1016/0956-7151\(94\)90502-9](http://dx.doi.org/10.1016/0956-7151(94)90502-9). <http://www.sciencedirect.com/science/article/pii/S0956715194905029>.
- [74] N. Stelmashenko, M. Walls, L. Brown, Y. Milman, Microindentations on w and mo oriented single crystals: an STM study, *Acta Metallurgica Materialia* 41 (10) (1993) 2855–2865. [http://dx.doi.org/10.1016/0956-7151\(93\)90100-7](http://dx.doi.org/10.1016/0956-7151(93)90100-7). <http://www.sciencedirect.com/science/article/pii/S0956715193901007>.
- [75] W. Poole, M. Ashby, N. Fleck, Micro-hardness of annealed and work-hardened copper polycrystals, *Scr. Mater.* 34 (4) (1996) 559–564. [http://dx.doi.org/10.1016/S1359-6462\(95\)00524-2](http://dx.doi.org/10.1016/S1359-6462(95)00524-2). <http://www.sciencedirect.com/science/article/pii/S1359646295005242>.
- [76] S. Suresh, T.-G. Nieh, B. Choi, Nano-indentation of copper thin films on silicon substrates, *Scr. Mater.* 41 (9) (1999) 951–957. [http://dx.doi.org/10.1016/S1359-6462\(99\)00245-6](http://dx.doi.org/10.1016/S1359-6462(99)00245-6). <http://www.sciencedirect.com/science/article/pii/S1359646299002456>.
- [77] J. Stölken, A. Evans, A microbend test method for measuring the plasticity length scale, *Acta Mater.* 46 (14) (1998) 5109–5115. [http://dx.doi.org/10.1016/S1359-6454\(98\)00153-0](http://dx.doi.org/10.1016/S1359-6454(98)00153-0). <http://www.sciencedirect.com/science/article/pii/S1359645498001530>.
- [78] N. Fleck, J. Hutchinson, A reformulation of strain gradient plasticity, *J. Mech. Phys. Solids* 49 (10) (2001) 2245–2271. [http://dx.doi.org/10.1016/S0022-5096\(01\)00049-7](http://dx.doi.org/10.1016/S0022-5096(01)00049-7). <http://www.sciencedirect.com/science/article/pii/S0022509601000497>.
- [79] U. Borg, C.F. Niordson, J.W. Kysar, Size effects on void growth in single crystals with distributed voids, *Int. J. Plast.* 24 (4) (2008) 688–701. <http://dx.doi.org/10.1016/j.ijplas.2007.07.015>. <http://www.sciencedirect.com/science/article/pii/S0749641907001003>.
- [80] L. Evers, W. Brekelmans, M. Geers, Non-local crystal plasticity model with intrinsic {SSD} and {GND} effects, *J. Mech. Phys. Solids* 52 (10) (2004) 2379–2401. <http://dx.doi.org/10.1016/j.jmps.2004.03.007>. <http://www.sciencedirect.com/science/article/pii/S0022509604000729>.
- [81] U. Borg, Strain gradient crystal plasticity effects on flow localization, *Int. J. Plast.* 23 (8) (2007) 1400–1416. <http://dx.doi.org/10.1016/j.ijplas.2007.01.003>. <http://www.sciencedirect.com/science/article/pii/S0749641907000083>.
- [82] O. Aslan, N. Cordero, A. Gaubert, S. Forest, Micromorphic approach to single crystal plasticity and damage, *Int. J. Eng. Sci.* 49 (12) (2011) 1311–1325 advances in generalized continuum mechanics A collection of studies in Engineering Sciences in memory of the late A.C. Eringen (1921–2009), <http://dx.doi.org/10.1016/j.ijengsci.2011.03.008>. <http://www.sciencedirect.com/science/article/pii/S0020722511000644>.
- [83] P. Franciosi, The concepts of latent hardening and strain hardening in metallic single crystals, *Acta Metall.* 33 (9) (1985) 1601–1612. [http://dx.doi.org/10.1016/0001-6160\(85\)90154-3](http://dx.doi.org/10.1016/0001-6160(85)90154-3). <http://www.sciencedirect.com/science/article/pii/0001616085901543>.